LAPPEENRANTA UNIVERSITY OF TECHNOLOGY
Department Of Technology
Master's Degree Programme in Technomathematics and Technical Physics

Fedyunina Olga

FOURIER SELF-DECONVOLUTION IN COHERENT ANTI-STOKES RAMAN SCATTERING SPECTRUM ANALYSIS

Examiners: Professor, Erik Vartiainen,

Professor, Erkki Lähderanta

Supervisor: Professor, Erik Vartiainen

ABSTRACT

LAPPEENRANTA UNIVERSITY OF TECHNOLOGY

Faculty Of Technology

Master's Degree Programme in Technomathematics and Technical Physics

Fedyunina Olga

(Fourier self-deconvolution in coherent anti-Stokes Raman scattering spectrum analysis)

Master's thesis

Year: 2009

54 pages and 32 figures

Examiners: Professor, Erik Vartiainen,

Professor, Erkki Lähderanta

Keywords: CARS, Fourier self-deconvolution, spectral analysis, coherent anti-Stokes Raman spectroscopy, wavelets.

Coherent anti-Stokes Raman scattering (CARS) microscopy is rapidly developing into a unique microscopic tool in biophysics, biology and the material sciences. The nonlinear nature of CARS spectroscopy complicates the analysis of the received spectra. There were developed mathematical methods for signal processing and for calculations spectra. Fourier self-deconvolution is a special high pass FFT filter which synthetically narrows the effective trace bandwidth features. As Fourier self-deconvolution can effectively reduce the noise, which may be at a higher spatial frequency than the peaks, without losing peak resolution. The idea of the work is to experiment the possibility of using wavelet decomposition in spectroscopic for background and noise removal, and Fourier transformation for line-narrowing.

Acknowledgements

First of all I wish to thank Professor Erik Vartiainen for his supervising me during researching, for his support and essential advices and help. Also I want to express a great acknowledgement to Erkki Lähderanta who rendered assistance me in studying in Lappeenranta University of Technology. I want to thank all the professors in Lappeenranta University and Professors of St. Petersburg Electrotechnical University who gave me an excellent basic knowledge which are essential and so necessary for my future job.

Especially I want to thank my parents who helped and inspired me.

Lappeenranta, May 2009.

Fedyunina Olga.

TABLE OF CONTENTS

Abbreviations

CARS	Coherent Anti-Stokes Raman Spectroscopy
SNR	signal-to-noise ratio
FFT	Fast Fourier Transformation
FWHH	Full width at half height
FSD	Fourier self-Deconvolution
P	dipole moment
$H_o(f)$	the actual spectrum
$N(f)$	noise
$H(f)$	the filtered spectrum
$G(f)$	the filter function
$g(t)$	the smoothing function
$\Pi_{2Ti}(t)$	a boxcar function
$W(f)$	instrumental function
$F\{Hw(f)\}$	The Fourier transform of the measured spectrum

Symbols

γ	the deconvolution filter
$\chi^{(1)}$	dielectric susceptibility
E	vibrational level energy
η	normal coordinate
Ω, ω	frequency [rad/s]
Δt	sampling interval
ϑ	the angle of the diffracted wave
ψ	full phase function or wavelet function [rad]
g	high-frequency components of wavelet decomposition
f	spectral component in low frequencies of wavelet decomposition

1. Introduction

1.1. Basic information about Raman spectroscopy

Raman spectroscopy is a spectroscopic technique used in condensed matter physics and chemistry to study vibration, rotational, and other low-frequency modes in a system [1]. It relies on inelastic scattering, or Raman scattering, of monochromatic light, usually from a laser in the visible, near infrared, or near ultraviolet range. The laser light interacts with phonons or other excitations in the system, resulting in the energy of the laser photons being shifted up or down. The shift in energy gives information about the phonon modes in the system. Infrared spectroscopy yields similar, but complementary, information.

Typically, a sample is illuminated with a laser beam. Light from the illuminated spot is collected with a lens and sent through a monochromator. Wavelengths close to the laser line, due to elastic Rayleigh scattering, are filtered out while the rest of the collected light is dispersed onto a detector.

Coherent anti-Stokes Raman scattering (CARS) microscopy is rapidly developing into a unique microscopic tool in biophysics, biology and the material sciences [1]. In analogy to spontaneous Raman scattering, CARS provides image contrast with chemical and physical specificity, without requiring any labeling of the specimen. It's specificity results from the fact that many of the important vibration spectral features remain resolvable even at room temperature and in samples as complex as live cells [2, 3]. In comparison to linear Raman scattering, however, the 3rd-order non-linear nature of CARS provides signal levels typically four orders of magnitude larger. Also, by virtue of the coherent nature of CARS, the signal is readily discriminated from background luminescence. This permits rapid image acquisition [4, 5] and - potentially - high speed time lapse vibration spectroscopic imaging with high sensitivity.

The rich informational content of vibration spectra is fully exploited in the multiplex CARS approach [6, 7], where a significant part of the vibration spectrum is acquired concurrently, and yielding high signal-to-noise ratio (SNR) vibration spectra at every point in the image. In addition, by dividing the measured multiplex CARS spectrum by a non-resonant reference spectrum, a "CARS signal strength" is obtained which is independent of experimental parameters such as laser power fluctuations or timing jitter.

1.2. Motivation of study

In spectroscopy a problem encountered again and again is the overlapping of spectral lines that are too wide compared with their interspaces. Therefore, ability to narrow spectral lines artificially would be very useful. For a line spectrum, such as a line narrowing is equivalent to resolution enhancement.

The nonlinear nature of CARS spectroscopy complicates the analysis of the received spectra. There were developed mathematical methods for signal processing and for calculations spectra. As a rule the mathematical methods include derivations, smoothing, deconvolution, background elimination ect.

Fourier self-deconvolution is a special high pass FFT filter which synthetically narrows the effective trace bandwidth features. This aids in identifying the principal bands that make up a more complex band with overlapping features. This can be useful for more accurate determination of the number of peaks in a trace region, the band positions, and areas. This technique can also be used to accurately determine starting parameters for applications such as Curve Fit. Two filters are employed in this method. An exponential filter is used to sharpen spectral features; the constant γ is varied to change the filter shape. The γ parameter equals the full width at half height (FWHH) of the widest resolvable peak. Realize that the imposed filter is the transform of a Lorentzian line shape.

As Fourier self-deconvolution tends to increase the apparent noise in the data, there is some benefit to be gained by simultaneously applying a low pass smoothing filter. This can effectively reduce the noise, which may be at a higher spatial frequency than the peaks, without losing peak resolution. The forms of the filters are boxcar and Bessel, and are mathematically described below.

The deconvolution filter is a simple exponential filter of the form $e^{2\pi\gamma X}$ where γ is the deconvolution filter constant and X is the array (i.e., data file) whose X range is normalized between 0 and 1. This function is multiplied by the Fourier transformed trace, and the data is then reverse Fourier transformed to give the result.

1.3. Aim of work

The main purpose for this Thesis is developing an algorithm of reducing the widths of spectral lines. This procedure is performed in the time domain. The idea of the work is to experiment the possibility of using wavelet decomposition in spectroscopic for background and noise removal, and Fourier transformation for line-narrowing

According to the aim it's necessary to solve the following problems:

- to study and analyze the methods of FSD and various methods of wavelets decompositions;

- to develop the algorithm reducing the widths of spectral lines and apply the method of spectroscopic de-noising

- to receive experimental measurements in coherent – Anti-Stokes Raman scattering spectrum of different substances;

- to apply the investigated method on our experimental measurements;

2. CARS spectroscopy

2.1. Raman scattering

Spontaneous Raman scattering is typically very weak, and as a result the main difficulty of Raman spectroscopy is separating the weak inelastically scattered light from the intense Rayleigh scattered laser light. Historically, Raman spectrometers used holographic diffraction gratings and multiple dispersion stages to achieve a high degree of laser rejection. In the past, PMTs were the detectors of choice for dispersive Raman setups, which resulted in long acquisition times. However, modern instrumentation almost universally employs notch or edge filters for laser rejection and spectrographs (either axial transmissive (AT), Czerny-Turner (CT) monochromator) or FT (Fourier transform spectroscopy based), and CCD detectors. There are a number of advanced types of Raman spectroscopy, including surface-enhanced Raman, tip-enhanced Raman, polarized Raman, stimulated Raman (analogous to stimulated emission), transmission Raman, spatially-offset Raman, and hyper Raman.

The Raman Effect occurs when light impinges upon a molecule and interacts with the electron cloud of the bonds of that molecule. The incident photon excites the molecule into a virtual state. For the spontaneous Raman scattering, the molecule will be excited from the ground state to a virtual energy state, and relax into a vibration excited state. Two series of lines exist around this central vibration transition. They correspond to the complimentary rotational transition.

Anti-stokes lines correspond to rotational relaxation whereas Stokes-Lines correspond to rotational excitation. A change in the molecular polarization potential — or amount of deformation of the electron cloud — with respect to the vibration coordinate is required for the molecule to exhibit the Raman effect. The amount of the polarizability change will determine the Raman scattering intensity, whereas the Raman shift is equal to the vibration level that is involved. The energy level diagram is showed in Fig. 1.

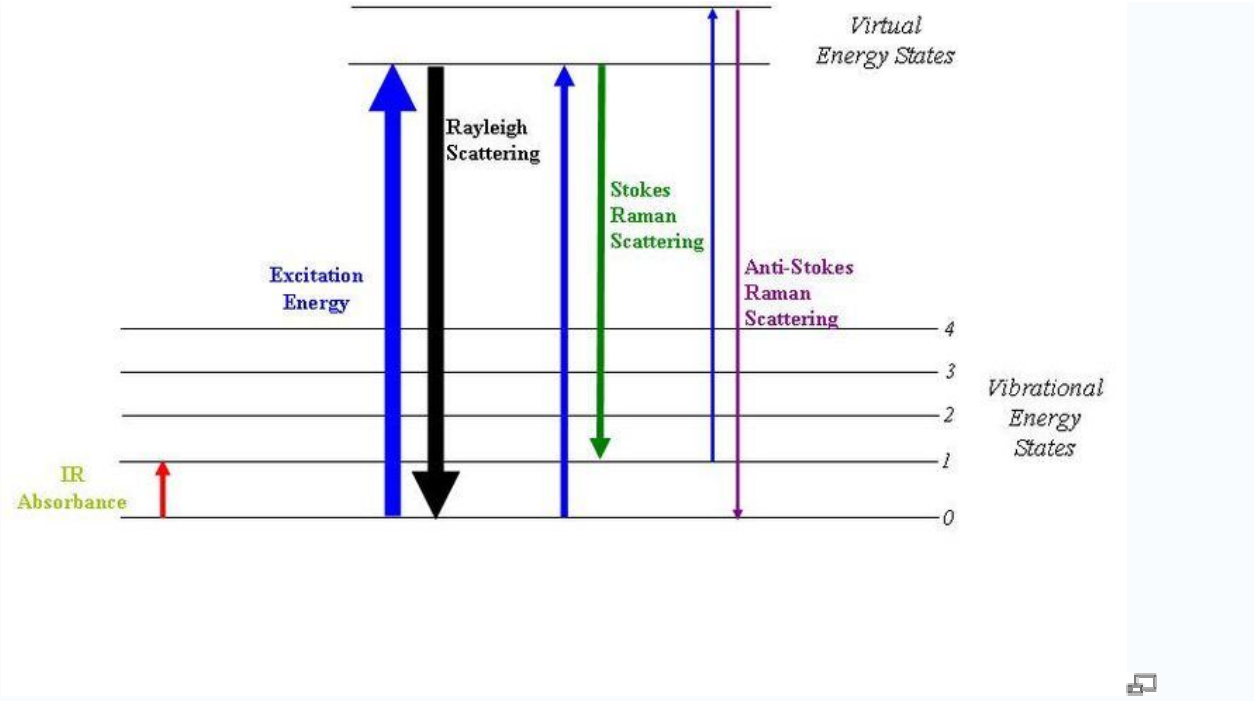

Figure 1. Energy level diagram showing the states involved in Raman signal. The line thickness is roughly proportional to the signal strength from the different transitions.

The frequency shifts of both Stokes and anti-Stokes components are equal and may be calculated by the following equation [1]:

$$\Delta V = (E_1 - E_2)/h, \quad (1)$$

where E_1 and E_2 are the energies of the high and low vibration levels. That allows investigating the vibration levels structure of a material by measuring of the Stokes or anti-Stokes shift. Because each substance has its own unique vibration levels structure the Raman scattering spectroscopy makes possible to determine the presence of some component in the medium.

2.2 Coherent anti-Stokes Raman scattering of light (CARS)

Due to the recent short-pulse laser technology developments, coherent anti-Stokes Raman scattering (CARS) microscopy is being used increasingly as a unique microscopic tool in biophysics, biology and the material sciences [8-10]. As a non-linear optical analogue of spontaneous Raman scattering, CARS potentially provides image contrast with chemical and physical specificity, since many of the important vibration spectral features remain resolvable even at room temperature and in samples as complex as live cells [8, 11, and 12].

Due to the coherent addition of both resonant contributions from different vibration modes and a non-resonant (NR) background contribution, CARS spectra generally have a complex shape. The influence of the NR background can be significantly reduced using various methods. One of them is a wavelet decomposition will be used in this thesis.

Coherent anti-Stokes Raman scattering is a nonlinear four wave mixing process. A general formulation of the reaction of matter on electric fields has been proposed by Bloembergen in 1965:

$$P = \chi^{(1)}E_1 + \chi^{(2)}E_1E_2 + \chi^{(3)}E_1E_2E_3 \qquad (2)$$

In linear optics the polarization P is linearly dependent on the electric field strength E_1, in optics this is of course the electric field strength of the light wave. The dielectric susceptibility $\chi^{(1)}$ corresponds to the dielectric constant. This linear part describes all aspects of linear optics like refraction, Rayleigh scattering, absorption (using a complex value for $\chi^{(1)}$) and even birefringence using a tensor notation for $\chi^{(1)}$. Strange enough non-linear optical effects have been known for more than a century, namely the Pockels (linear electro-optic) effect and the Kerr (quadratic electro-optic) effect. However, with these effects one "cheats" the above formula by replacing one or two of the E fields by externally applied static electric fields. Doing so, easily fields of 1 to 20 kV/cm can be applied to matter. This "compensates" then for the extremely low values of the $\chi^{(i)}$. In contrast, the electric field of sun light is just about 6 V/cm. This explains why non-linear optical effects are not discernible in daily life.

Things change dramatically when using lasers as light sources. CW laser beams can be focused to spots in the micrometer range. The coherence of the light allows for long interaction lengths.

Pulsed lasers easily reach intensities of 10^8 W/cm^2, when focused even 10^{12} W/cm^2. When using focused radiation of a pulsed laser, non-linear optical effects get comparable to linear optical effects.

From the laws of goniometric multiplication it is obvious that the second term in (2) leads to sum and difference frequency generation and especially to frequency doubling. The latter is commonly used in many types of laser systems, as is the Pockels effect. However, these effects need a "built-in" anisotropy of matter, usually only found in asymmetric crystals (phosphates, borates, arsenates, "KDP", and such). Actually these effects could be looked at as chi-three effects with a built-in DC electrical field strength. For gases there will be no "chi-two" effects owing to their inherent isotropy.

The third term, "chi-three", does not need an anisotropy. It is always present, although it may be very small, but never equals zero. This holds not only for molecular gases but also for atomic gases and even for vacuum. This omnipresence of the $\chi^{(3)}$ term is one of the main problems with CARS spectroscopy. The $\chi^{(3)}$ containing term results in frequency combinations of three incoming waves, e.g. $\omega_1 + \omega_2 + \omega_3$, $2\omega_1 + \omega_2$, $3\omega_1$, $2\omega_1 - \omega_2$, the latter being the CARS process.

Spontaneous Raman scattering of light is connected with thermal oscillations of molecules. It is a corollary of violation of a principle of superposition. Light waves and oscillations of a medium produce mutual influence against each other [13]. Raman spectroscopy studies the modulation of light by thermal (spontaneous) oscillations of molecules. It would be natural to expect a boomerang effect of action of light waves on molecular oscillations. The reason of inverse action of the light waves on molecular oscillations is dependency $\chi(\eta_i)$. When a molecule gains a dipole moment in a field of a light wave, it starts to co-operate with the wave. The energy of this interaction is

$$W = -PE = -\chi(\eta_i)E^2 \qquad (3)$$

Thus the force starts to act on the molecule:

$$F = -dW/d\eta_i = (d\chi/d\eta_i)E^2 \qquad (4)$$

If two light waves (E_1 and E_2) are spread simultaneously in a medium and they have frequencies ω_1 and ω_2, then the field $E = E_1 + E_2$ and the force F will contain, in particular, a component varying with frequency $\omega_1 - \omega_2$. Usually waves E_1 and E_2 are the waves of visible range. Nevertheless it is possible to

make the difference $\omega_1-\omega_2$ very small, and in particular close to the frequency of normal oscillation: $\omega_1-\omega^2 = \Omega_j$. The resonance swing of oscillations of atoms in molecules is possible in that case. In these conditions regular forced oscillations are superimposed on random molecular movement. The phases of these forced oscillations in various molecules are determined by phases of forcing fields E_1 and E_2. Having directed to such medium a probe wave with frequency ω, it is possible to observe Stokes and anti-Stokes waves with frequencies

$$\omega_{s.\,a.} = \omega \pm (\omega_1 - \omega_2) \tag{5}$$

Effectiveness of energy exchange between interacting waves, as at any resonance, depends on phase relations between them. Therefore the scattered wave will have the greatest intensity in the certain directions along which phase relations between spread waves are kept. These directions are set by conditions of phase synchronism:

$$k_{s.\,a.} = k \pm (k_1 - k_2) \tag{6}$$

$k_{s.\,a.}$, as is the wave vector of Stokes and anti-Stokes waves, k_1, k_2, k_3 are the wave vectors of the probe wave and pump waves accordingly. A corollary of this is the narrow directness of the scattered wave that allows to collect the scattered radiation almost completely and to direct it to a photo detector .The anti-Stokes scattering is considered to be the most interesting, as in anti-Stokes area; for example, there is no luminescence of a sample. The energy diagram is shown in Fig. 2.

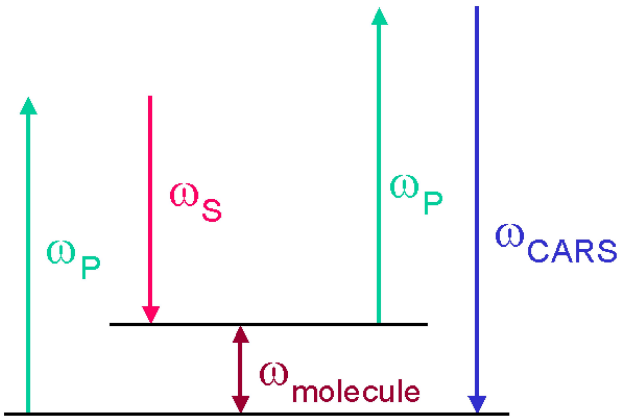

Figure 2. The energy scheme of CARS. ω_p is the frequency of a pump field, ω_s is the frequency of a Stokes field, $\omega_{molecule}$ is the frequency of natural oscillations of a molecule, ω_{CARS} is the frequency of a probe field [14].

It is natural, that scattering on the phase matching oscillations will lead to significant growth of intensity of the scattered light. It achieves 1% from intensity of the probe wave. It is necessary to underline, that so effective scattering is a corollary first of all phase matching or coherence of forced oscillations,

instead of their big amplitude. The spectrum of a coherent scattering can be received, if there is a possibility of smooth frequency tuning of the pump waves. he interesting singularity of the CARS signal is exhibited. Radiation, which is coherently scattered by molecules on frequency ω_a, consists of two components: the resonant component connected with oscillations of molecules, and the *non-resonant* component which is not connected with molecular oscillations. The second component practically does not depend on the difference in frequencies of the pump waves. As these components are coherent, they interfere among themselves and in a registered signal there are characteristic maxima and minima of intensity at scanning the difference in frequencies near to frequency of a molecular resonance. Therefore the form of the line shape of molecular oscillations in spectroscopy CARS strongly differs from the form of a spontaneous Raman spectroscopy line [15].

3. Processing of signal and spectrum

3.1 Mathematical filtering and smoothing

Mathematical filtering

A measured spectrum generally contains undesired components, noise, in addition to the actual spectrum. The measured spectrum is $H_0(f) + N(f)$, where $H_o(f)$ is the actual spectrum and $N(f)$ is noise.

Band limited while noise consists of noise at all frequencies in a limited hand, below a maximum frequency f_{noise}. If the maximum frequency of the actual signal is f_{max}, we have

$$\begin{cases} H_0(f) = 0, & |f| \geq f_{\max}, \\ N(f) = 0, & |f| \geq f_{\text{noise}}. \end{cases} \tag{7}$$

Figure 3 [16] shows an example of a spectrum which contains band limited while noise. In this example, the maximum frequency of the noise f_{noise}=3 f_{max}

The registered signal which gives the noisy spectrum is $h_0(t) + n(t)$, where h_0 is the actual signal and $n(t)$ the noise. Figure 4 shows such a signal [16].

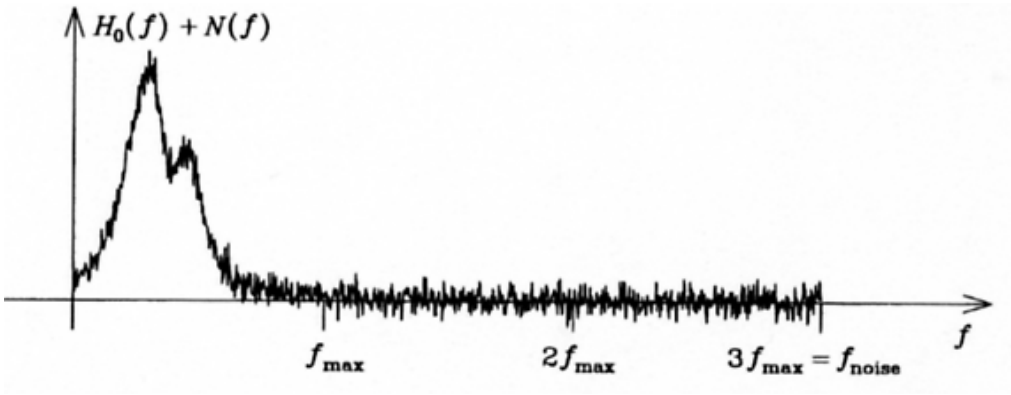

Figure 3. A spectrum $H_0(f) + N(f)$, consisting of the actual spectrum $H_0\{f\}$ and noise $N\{f\}$. $H_0\{f\} = 0$ at $|f| > f_{max}$,, and the band limited while noise $N(f) = 0$ al $|f| > f_{noise}$.

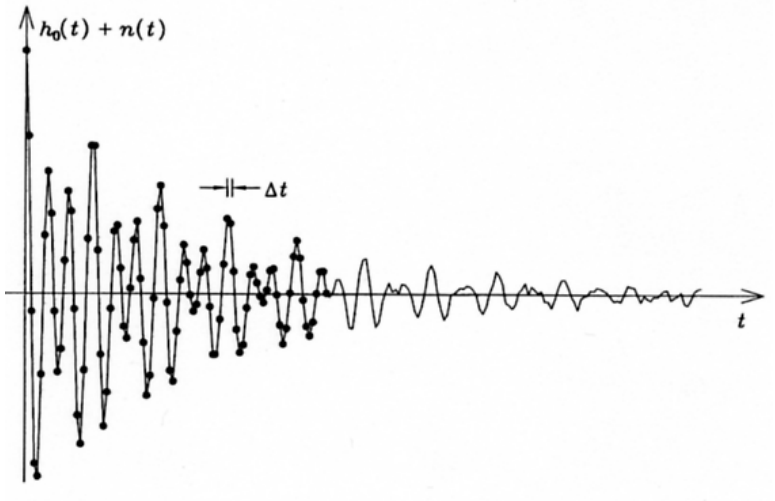

Figure 4. A registered signal $h_0(t) + n(t)$, where $h_0(t)$ is the actual signal and $n(t)$ is contribution of noise in the signal. Δt *is* the sampling interval.

If we know that the maximum frequency of the spectrum is f_{max}, then a natural choice for the sampling interval would be $\Delta t = 1/(2 f_{max})$, because then the spectrum would not be aliased. However, if $f_{noise} > f_{max}$, then noise will be aliped, and the amplitude of noise in the spectrum will grow. In the case of Figure 3, where $f_{noise} = 3 f_{max}$, the amplitude of noise in the spectrum would grow √3 -fold due to aliasing. Generally, if $f_{noise} = n f_{max}$, then the sampling interval $\Delta t = 1/(2 f_{max})$ increases the amplitude of the noise √n-fold.

The aliasing of noise can be avoided by using the shorter sampling interval

$$\Delta t = 1 / 2f_{noise} \quad (8)$$

but then the number of data increases. In the example of Figure 3, we would have $\Delta t=1/ (6 f_{max})$, and the number of data would be increased 3-fold.

An alternative solution for the elimination of high-frequency noise is low-pass filtering. Low-pass filtering is a special case of *bund-pass filtering,* which filters away all other frequencies of the spectrum than the desired bands containing information.

Let us examine a spectrum $H(f) = Ho(f) + N(f)$, which consists of an actual spectrum $Ho(f)$ limited to a band $f_a < f < f_b$, and of band limited white noise $N(f)$ at frequencies $f < f_{noise}$. Figure 5 shows an example of such a spectrum. The filtered spectrum of $H(f)$ is

$$H'(f) = G(f) H(f), \quad (9)$$

where the *filter function,* or the *transfer function, G(f)* is

$$G(f) = \begin{cases} 1, & f_a \le |f| \le f_b, \\ 0, & |f| < f_a, \text{ or } |f| > f_b, \end{cases} \quad (10)$$

which is shown in Figure 6.

Taking the Fourier transforms of both sides of Equation 2.5 and applying the convolution theorem we obtain

$$F\{H'(f)\} = F\{G(f)\} * F\{H(f)\} \quad (11)$$

or

$$h'(t) = g(t)*h(t) \quad (12)$$

where $h(t) = ho(t) + n(t)$ is the signal which corresponds to the unfiltered spectrum, $h'(t)$ is the signal which corresponds to the filtered spectrum, and $g(t) = F\{G(f)\}$ is the *smoothing function,* or the *impulse response.* $h'(t)$ is called a *smoothed* signal. We can compute $g(t)$ using the shift theorem or the modulation theorem, and obtain

$$g(t) = 2(f_b - f_a) \text{ sinc } [n(f_b - f_a)t] \cos [\pi(f_b + f_a)t] \quad (13)$$

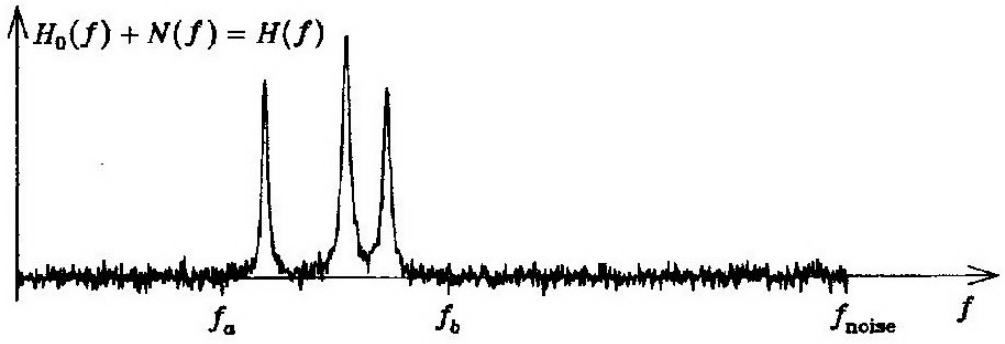

Figure 5. A spectrum *H (f)* — $W_o(/)$ + *N(f),* which consists of an actual spectrum *Ho(f)* limited to a band $f_a < f <- f_b$ and of band limited while noise *N{f)* at frequencies $f < f_{noise}$. The mirror image *H (—f) = H (f)* is not shown in the figure.

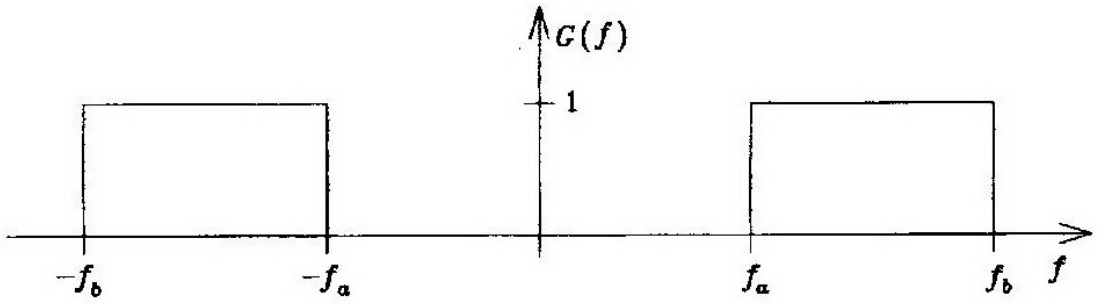

Figure 6. The transfer function *G{f)* for band-pass filtering of the spectrum shown in Figure 5.

Mathematical smoothing

A measured spectrum often consists of spectral lines, which have a certain line shape, and of white noise. Such a spectrum is illustrated in Figure 7. *Smoothing* of a spectrum *H(f)* is an operation where the spectrum is convolved with a smoothing function *W(f)* in order to reduce the rapidly oscillating random noise of the data[16].

A spectrum with noise can be written as *H (f) = Ho (f) + N (f),* where *Ho (f)* is the true spectrum and *N(f)* is the while noise spectrum. The smoothing operation in the frequency domain can be expressed as

$$H'(f) = G(f) * H(f) \tag{14}$$

where *H'(f)* is the smoothed spectrum.

According to the convolution theorem, the Fourier transform of a convolution is a simple multiplication. Consequently, convolution of a spectrum in the frequency domain is the same as multiplication of a signal in the time domain:

$$F\{H'(f)\} = F\{W(f)\} * F\{H(f)\} = A(t)h(t) \tag{15}$$

A{t) = F{W(f)} is the weight function, by which the original signal *h(t) = F{H(f)}* is multiplied. This operation can be regarded as filtering of the signal. Smoothing of a spectrum corresponds to filtering of the signal, in the same way as filtering of a spectrum corresponds to smoothing of the signal.

Multiplication of the signal *h (t) = F {H(f)}* by the weight function *A{t) = F{W(f)}*is the same operation as is performed in the apodization method.

The aim of smoothing is to enhance the signal-lo-noise ratio *(S/N)* by reducing the noise as much as possible, but distorting the true spectral line shape as little as possible.

The simplest way of smoothing a spectrum is the simple truncation of the signal. This makes sense, because the ratio of true information and noise is generally the best near *t* = 0, and the worst al large values of *t.* In truncation, the signal *h(t)* is multiplied by a boxcar function

$$\Pi_{2T_i}(t) = \begin{cases} 1, & |t| \leq T_i, \\ 0, & |t| > T_i. \end{cases} \tag{16}$$

Multiplication by a boxcar function is the weakest form of apodization which does not modify the signal or the noise in the retained portion of the signal.

An *optimal smoothing* is achieved, if the signal is truncated al such a point *Ti* beyond which all information *h{t)* disappears under the noise *n(t).* This is illustrated in Figure 2.10. At the point *Ti the* rms. or the root mean square, of the noise

$$\sqrt{\overline{n^2(t)}} = \sqrt{\lim_{T\to\infty} \frac{1}{2T} \int_{-T}^{T} n^2(t)\, dt} \tag{17}$$

is equal to the amplitude of the signal.

The signal of an optimally smoothed spectrum is

$$h'(t) = \Pi_{2Ti}(t)\, h(t) \tag{18}$$

and consequently, the optimally smoothed spectrum is

$$H'(f) = F^{-1}\{\Pi_{2Ti}(t)\, h(t)\} = F^{-1}\{\Pi_{2Ti}(t)\} * H(f) = 2T_i\, sinc(2\pi f T_i) * H(f) \tag{19}$$

We can see that the smoothing function *W (f)* of the spectrum is a sin function [16].

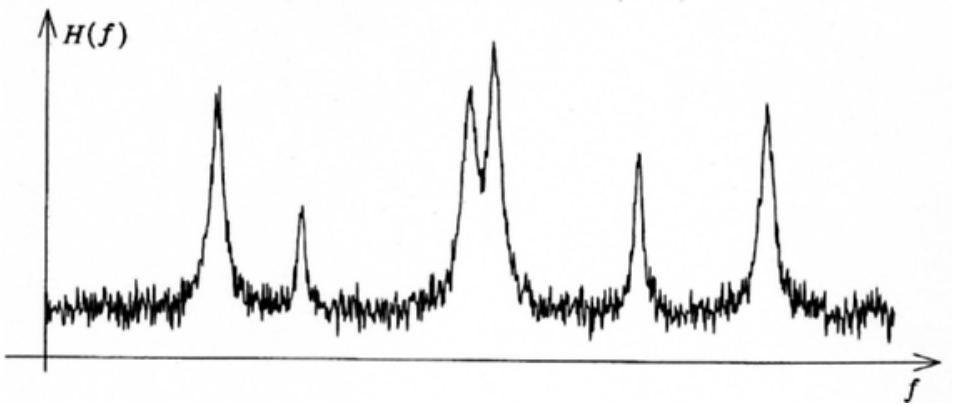

Figure 7. A spectrum which consists of spectral lines and white noise

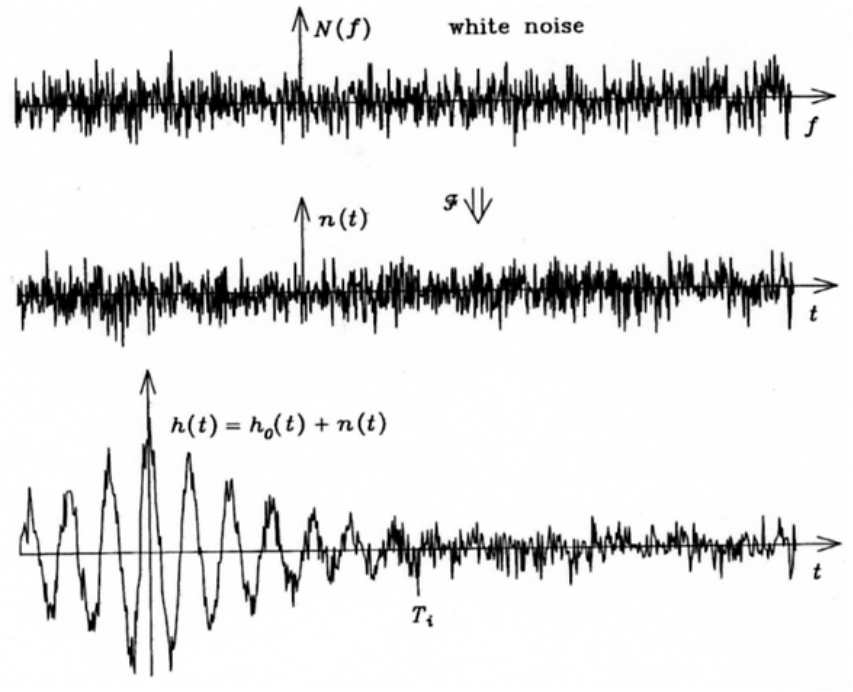

Figure 8. White noise spectrum *N(f)* in *f*-domain, white signal noise n(t) = *F{N(f)}* in *t*-(domain. and the noise-corrupted signal *h(t) = h0(t)+n(t)*. Beyond the point *T,* all information *h0(t)* disappears under the noise *n{t)*

Figure 9 [16] shows a simulation of a smoothing operation. In practice, it is impossible to carry out sine smoothing in the frequency domain exactly, because the convolution has to be truncated. The optimal smoothing is much easier to perform in the time domain. This is both fast and accurate.

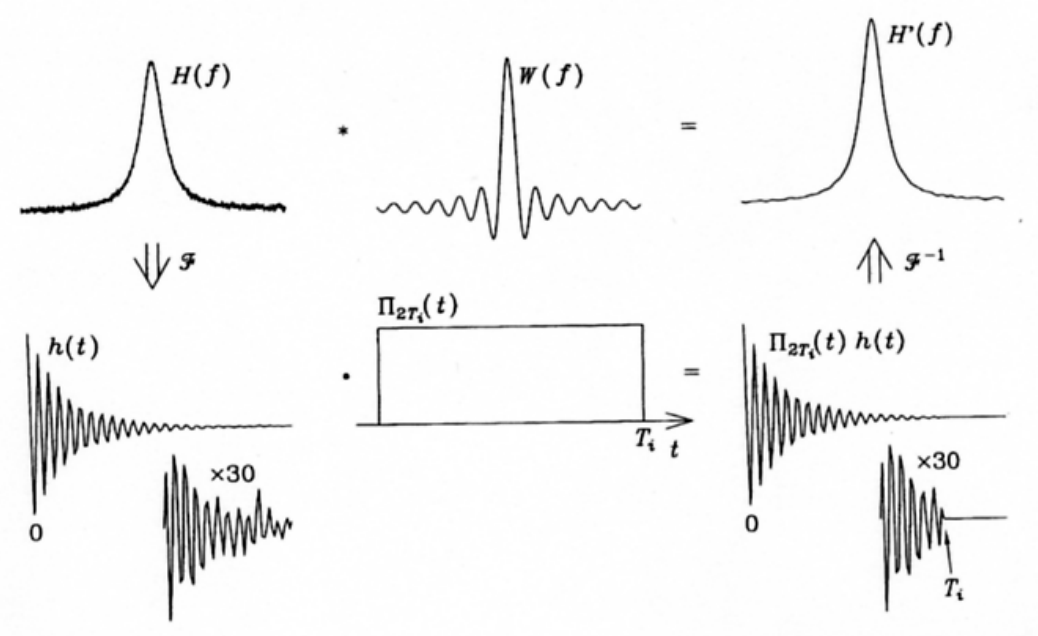

Figure 9. The spectrum *H(f),* which has a signal-to-noise ratio of 20 can be smoothed to the spectrum *H'(f)* by two alternative procedures. In the first procedure, the smoothed spectrum is obtained by convolving the original - spectrum by a smoothing function *W(f),* which in this simulation is a sin function. This is a laborious, procedure. In the second procedure the spectrum is Fourier transformed into the signal *h(t)=F{H(f)},* and multiplied by a boxcar function Π2Ti(t). The smoothed spectrum is obtained as the inverse Fourier transform of the product Π2Ti(t)h(t). The walk portions of the signal are shown 30-fold magnified around *Ti.*

3.2. Elimination of background

A spectrum *H (f)* often contains a slowly varying background. In the signal *h(t)* the background information is near $t = 0$. Consequently, the background can be eliminated by suppressing the beginning of the signal. This process is shown in Fig. 10. If the FWHM of the background is $\Delta f0$, then the background disappears, if the values of the signal are replaced by zero at $|t| < 1.21/(2\,\Delta f0)$.

The removal of part of the signal causes a distortion of spectral lines. The broadest spectral lines experience the largest distortion. The maximum relative distortion of a spectral line with FWHM A*f*, due to the shortening of the significant part of the signal, is approximately *Δf /(Δf0)*. The relative distortion of narrow spectral lines is smaller than this.

In practice, the distortion of the spectral lines due to the elimination of the background is often smaller than the noise of the spectrum. However, in some cases the background of the measured spectrum cannot be considered slowly varying. If the derivative of the background is large at some points, then the background cannot be eliminated from the whole spectrum. We may eliminate it part by part from those areas where it is slowly varying, and process the areas with high background derivative in some other way.

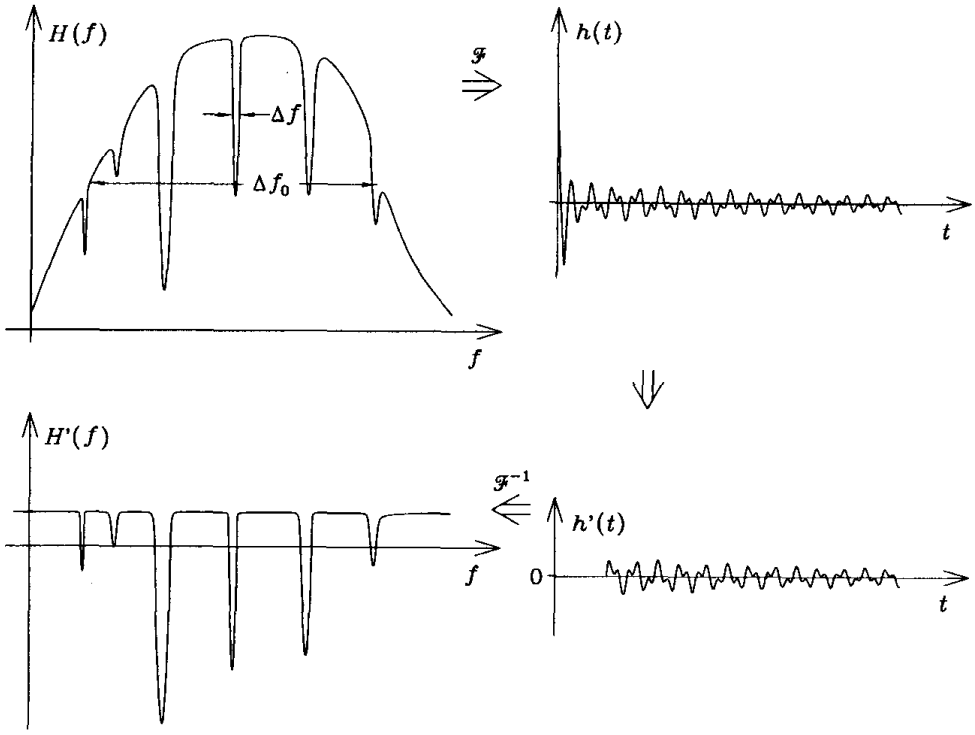

Figure 10. The background of the spectrum *H(f)* may be eliminated by first taking the Fourier transform of the spectrum *F{H(f)} = h(t),* and then replacing the values of the beginning of the signal *h(t)* by zero. The inverse Fourier transform of the manipulated signal *h'(t)* gives a spectrum *H'(f)* without the background: $F^{-1}\{h'(t)\}=H'(f)$ [16].

3.3. Deconvolution

Deconvolution is the inverse operation of convolution. Let us assume that an observed spectrum is

$$H_w(f) = W(f) * H(f) = \int W(f')H(f - f')df' \quad (20)$$

where *H(f)* is the real spectrum, and *W(f)* an instrumental function, due to the measurement system. The true spectrum may be computed from the measured spectrum by deconvolution, if the instrumental function is known.

Deconvolution in the frequency domain is a very difficult operation. An easier way is to perform the operation in the time domain. If we take Fourier transform of both sides of Equation 2.33, and apply the convolution theorem, we obtain

$$F\{H_w(f)\} = F\{W(f)\}\, F\{H(f)\} \quad (21)$$

Consequently, the original spectrum can be expressed as

$$H(f) = \mathcal{F}^{-1}\{\mathcal{F}\{H(f)\}\} = \mathcal{F}^{-1}\left\{\frac{\mathcal{F}\{H_W(f)\}}{\mathcal{F}\{W(f)\}}\right\}, \quad (22)$$

If F {W(f)} ≠ 0 at every value of *t.*

We can see that deconvolution is possible only if *F{W(f))* ≠ 0 at every value of *t.* The validity of this condition is, however, difficult to observe in *f*-domain! In practice, the noise of the measured spectrum *Hw(f)* will limit the use of deconvolution, since the noise will "explode" at the points where *F{W(t))* is close to zero. This can be avoided by smoothing the spectrum. We can use the optimal smoothing, and multiply the signal in *t*-domain by a boxcar function $\Pi_{2Ti}(t)$ (Equation 16). As demonstrated in Figure 11 [16], we can choose the point T_i; in such a way that at this point the value of the signal $\approx \sqrt{n^2(t)}$ that is, behind T_i the signal *F{W(f)}* is smaller than noise.

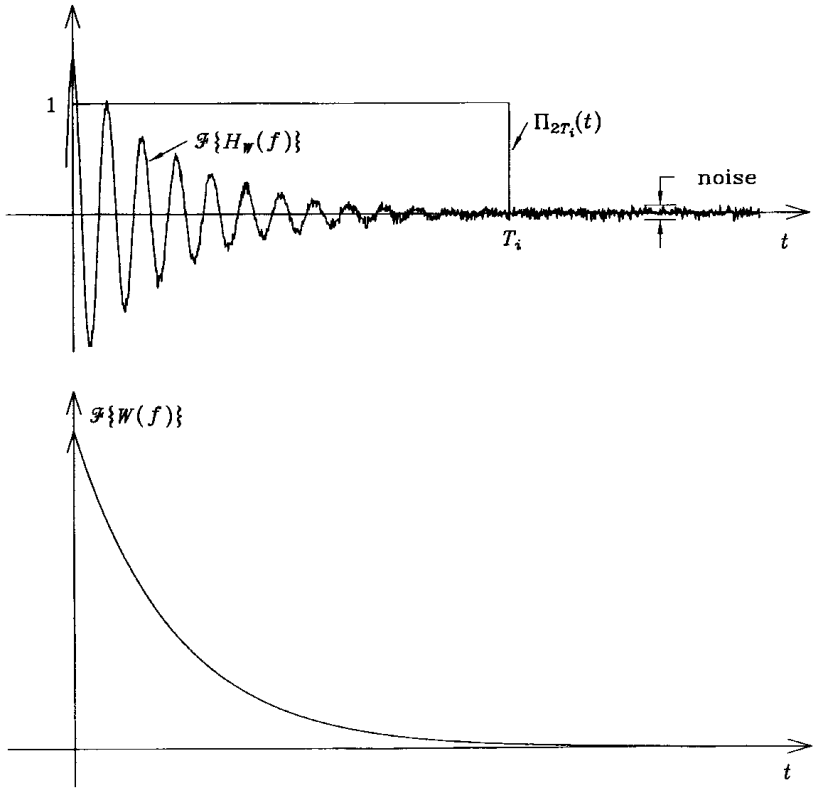

Figure 11. The Fourier transform of the measured, spectrum *F{Hw(f)},* and the truncation boxcar function Π*2Ti(t)*.Behind the point *Ti* the signal *F{Hw(f)*} is mostly noise. The lower curve is the Fourier transform of the instrumental function *F{W(f)*}

The deconvolution of the smoothed measured spectrum $H^S w(f)$ gives

$$H^{\mathrm{S}}(f) = \mathcal{F}^{-1}\left\{\frac{\mathcal{F}\{H_W^{\mathrm{S}}(f)\}}{\mathcal{F}\{W(f)\}}\right\} = \mathcal{F}^{-1}\left\{\frac{\Pi_{2T_i}(t)\mathcal{F}\{H_W(f)\}}{\mathcal{F}\{W(f)\}}\right\}, \tag{23}$$

Because

$$H^S_w\,(f) = F^{-1}\,\{\Pi_{2Ti}(t)\} * H_w(f) \tag{24}$$

From Equations 23 and 22 we obtain

$$H^S\,(f) = F^{-1}\,\{\Pi_{2Ti}(t)\} * H(f) \;= 2T_i\,sinc(\pi f T_i) * H(f) \tag{25}$$

If the Fourier transform of the instrumental function *F{ W(f})* equals zero behind a certain value of *t* (or at certain values of *t),* then the undistorted spectrum cannot be computed exactly by deconvolution, or by any other means, even if there would be no noise. This is natural, because

in the area where $F\{W(f)\}=0$ the undistorted signal $F\{H(f)\}$ is multiplied by zero and is permanently lost.

Let us examine, as an example, a grating. The instrumental function or the convolving function $W(v)$ of a grating, in the wave number domain

$$W(\upsilon) \propto L\, sinc^2(\pi\upsilon L) \tag{26}$$

where

$$L = Nd \sin\theta \tag{27}$$

Here N is the number of slits in the grating, d is the distance of the slits, and ϑ *is* the angle of the diffracted wave. If the true spectrum is $H(v)$, then the measured spectrum is the convolution $Lsinc^2(\pi vL)*H(v)$. The Fourier transform of this is the measured signal $F\{L\, sinc^2(\pi vL)\}F\{H(v)\}$. On the other hand, we know that $F\{L\ \mathrm{sinc}^2(\pi vL)\}$ is the triangular function shown in Figure 12. Consequently, a grating loses information $h(x)$ in the area where $|x| > Nd \sin\vartheta$.

Generally, the aim of deconvolution is to compute the true spectrum $H(f)$ from the measured spectrum $Hw(f)$, that is, to correct the distortion caused by the instrumental function $W(f)$, which generally is known. This is usually successful, especially, if the instrumental function is much narrower than the spectral lines. This situation is illustrated in Figure 13 [16].

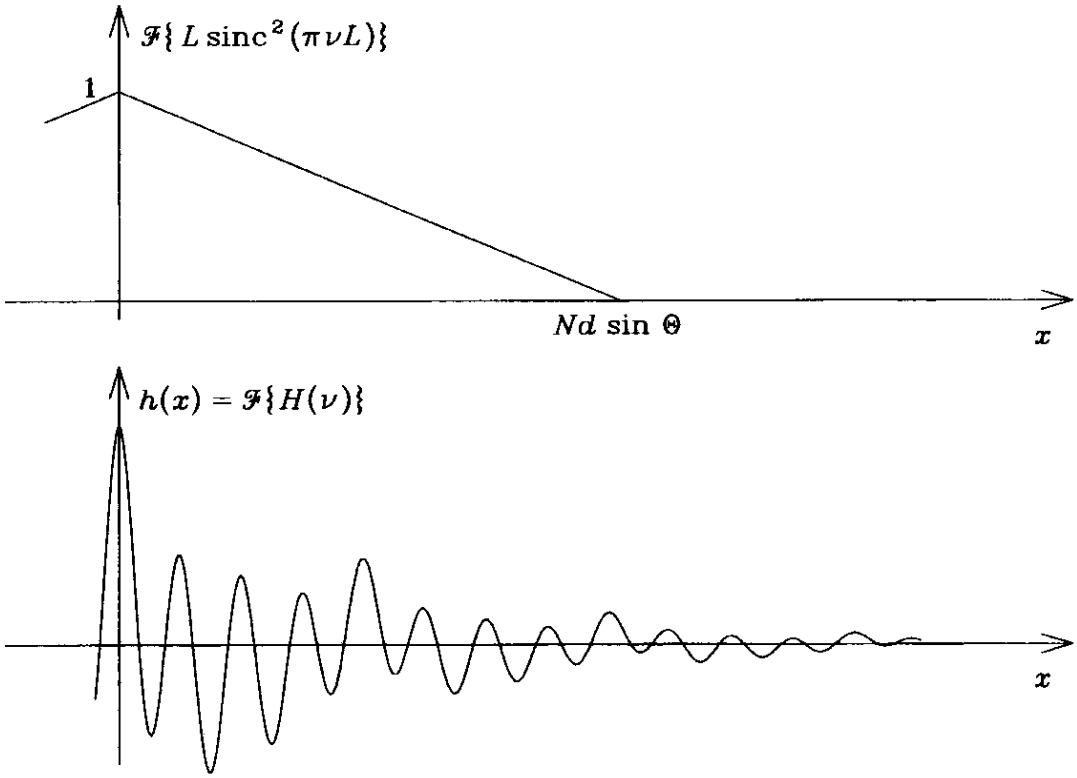

Figure 12. The Fourier transform of the instrumental function *F{L sinc^2(πνL)}* and the true signal *h(x) =F{H(ν)}.* The measured signal is the product of these two functions

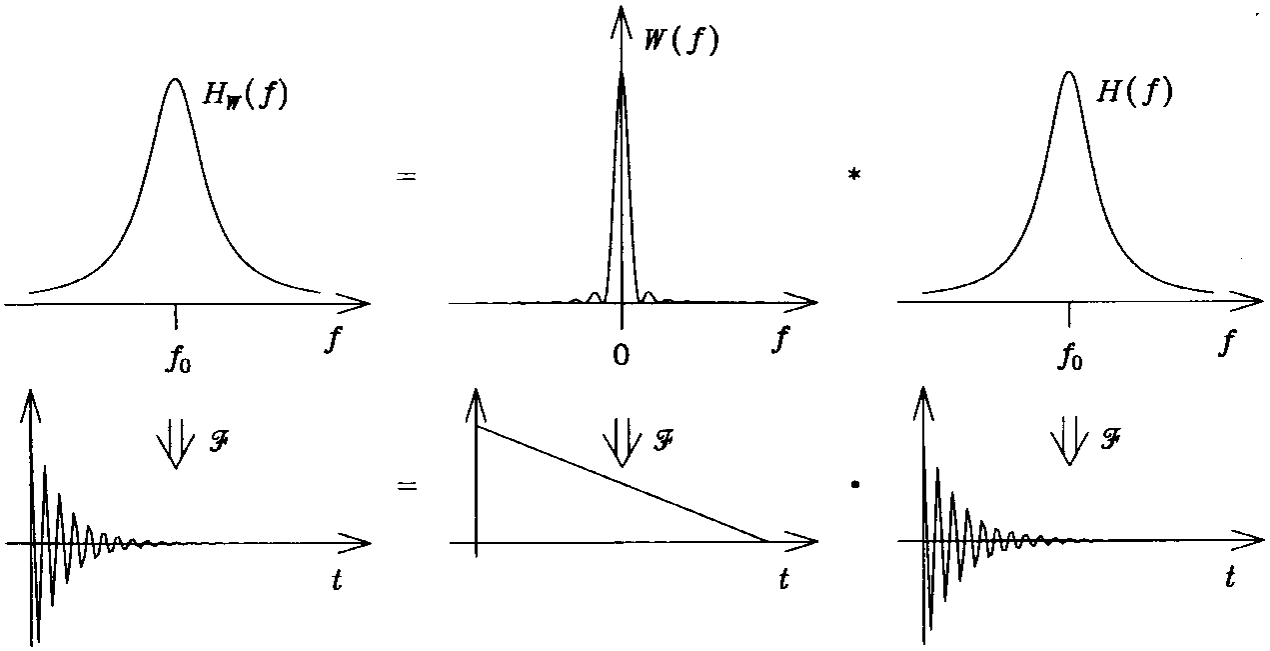

Figure 13. If the instrumental function *W(f)* has a small FWHM, then it distorts the spectral lines of (he true spectrum *H(f)* only slightly, and the measured spectrum *Hw(f) ≈ H(f)*

4. The main principles of Fourier self-deconvolution

4.1 The main principle of FSD

Narrowing a spectral line in the spectral domain is equivalent to stretching the corresponding signal, the decaying wave, in the signal domain. Making the decaying wave decay more slowly in f-domain results in a narrower line in *t*-domain. This operation can be done by dividing the wave by some smoothly decaying curve. In the spectral domain this operation appears as deconvolution. In the same way as convolution always broadens spectral lines, its inverse operation, deconvolution, always narrows the lines [16].

In *Fourier self-deconvolution,* FSD, the spectrum is deconvolved by the line shape of the spectrum itself. The line shape is a line situated in the origin, and it has an area equal to one. In FSD, the signal in f-domain is divided by the Fourier transform of the line shape function. A return to *t*-domain by inverse Fourier transform gives a spectrum with narrower spectral lines. The goal of FSD is to enhance the spectral resolution, that is, make the spectral lines narrower, by mathematical means, in such a way that the frequency and the integrated intensity of each line are preserved.

Let us assume that we recorded the line shape $W_R(f)$. We remember that we can write $W_R(f) = W_R(f) * \delta(f)$. If we carry out deconvolution of $W_R(f)$ by the line shape $W_R(f)$ itself, Equation 2.35 gives

$$\mathcal{F}^{-1}\left\{\frac{\mathcal{F}\{W_R(f)\}}{\mathcal{F}\{W_R(f)\}}\right\} = \mathcal{F}^{-1}\{1\} = \delta(f), \tag{26}$$

and the result is Dirac's delta function. Total removal of the original line shape results in infinitely narrow lines. In practice, however, we obtain a sine function, which originates from the inevitable truncation of the now non-decaying wave. In addition, the noise of the original spectrum as well as the highly oscillating sine line requires smoothing. The spectrum should be apodized by some window function in order to make the spectral lines smoother.

Let us assume that a registered spectrum $H_R(f)$ consists of lines $A_i W_R(f — fi)$:

$$H_R(f) = \Sigma A_i W_R(f-f_i) \tag{27}$$

where A_i is the area (intensity), and f_i the position of the i-th line. $W_R\{f\}$ is the line shape function of the registered spectrum. The area of $W_R(f)$ is equal to one. We are assuming that all the lines have this same line shape. The Fourier self-deconvolved spectrum $H_{FSD}(f)$ can then be expressed as

$$H_{\mathrm{FSD}}(f) = \mathcal{F}^{-1}\left\{\frac{\mathcal{F}\{W(f)\}\mathcal{F}\{H_{\mathrm{R}}(f)\}}{\mathcal{F}\{W_{\mathrm{R}}(f)\}}\right\}, \tag{28}$$

where $W(f)$ is the smoothing function, which is also the desired new line shape. The area *of* $W[f]$ is equal to one. In t-domain $F\{W\{f\}\}$ is the window function by which the signal is apodized in order to smooth the spectrum.

Since deconvolution is equivalent to division in t-domain, it is clearly a linear operation. Deconvolving a linear combination of spectral lines of various heights simultaneously gives the same result as deconvolving each tine separately, providing that they have a common line shape. The relative heights of the lines remain unchanged. Since the shift theorem states that shifting a line in f-domain corresponds lo multiplication by an exponential wave in t-domain, the positions of the lines may also be arbitrary. FSD is able to narrow an overlapping set of an unknown number of spectral lines without the need to know their heights and positions.

Since the operation is linear, we can examine only one spectral line. A registered spectrum with one spectral line can be written as

$$H_R(f) = A_0 W_R(f-f_0) \tag{29}$$

By applying the shift theorem, we obtain that the new spectrum after FSD is

$$\begin{aligned} H_{\mathrm{FSD}}(f) &= \mathcal{F}^{-1}\left\{\frac{\mathcal{F}\{W(f)\}\mathcal{F}\{A_0 W_{\mathrm{R}}(f-f_0)\}}{\mathcal{F}\{W_{\mathrm{R}}(f)\}}\right\} \\ &\overset{\dagger}{=} \mathcal{F}^{-1}\left\{\frac{\mathcal{F}\{W(f)\}A_0\mathcal{F}\{W_{\mathrm{R}}(f)\}e^{i2\pi f_0 t}}{\mathcal{F}\{W_{\mathrm{R}}(f)\}}\right\} \\ &\overset{\dagger}{=} \mathcal{F}^{-1}\{\mathcal{F}\{A_0 W(f-f_0)\}\} = A_0 W(f-f_0). \end{aligned} \tag{30}$$

We can see that FSD is, indeed, the operation

$$A_0W_R(f\text{-}f_0) \rightarrow A_0W(f\text{-}f_0) \tag{31}$$

A registered spectral line of the shape $W_R(f)$ is turned into a narrower spectral line of the shape $W(f)$, the area and the position remaining unchanged.

The principle of the FSD procedure is illustrated in Figure 14**.** The registered line is deconvolved by its own line shape by division by $F\{Wn(f)\}$ in t-domain, resulting, in the absence of truncation, in Dirac's delta function $A0\delta(f - f0)$. This Dirac's delta function is smoothed by multiplication by $F\{W\{f)\}$ in t-domain, resulting in the final line shape $W(f)$.

We must, however, remember, that in practice the line shape $W_R(f)$ of a registered spectrum is not the true original line shape, but the convolution of the instrumental function of the measurement system $W_{inst}(f)$ and the true line shape $W_{true}(f)$, as illustrated in Figure 15.

The main goal of FSD is lo reduce the half-widths of the spectral lines. The efficiency of [his is given by the *resolution enhancement factor*

$$K = \frac{\sigma_R}{\sigma} = \frac{\text{FWHM of the registered line}}{\text{FWHM of the smoothing function}}. \tag{32}$$

This may be simply called the K-value.

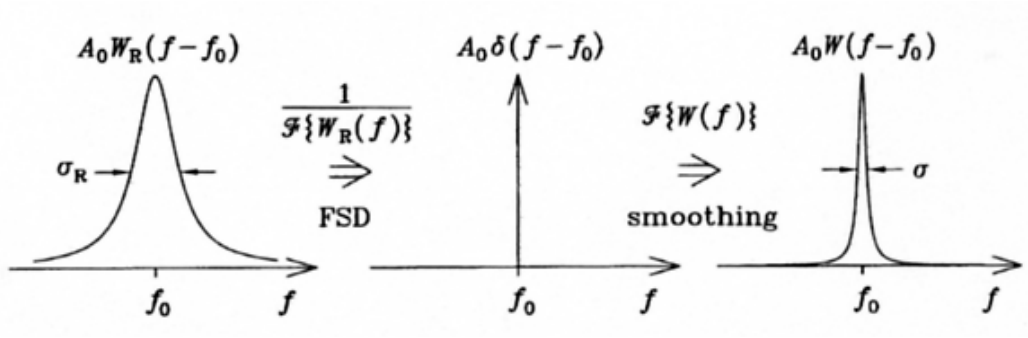

Figure 14. The procedure of FSD. The registered spectral line $A0W_R(f - f0)$ is Fourier self-deconvolved, resulting in Dirac's delta peak $A_0\delta(f - f_a)$, and then smoothed. resulting in the final line $A0W(f - f_0)$ [16].

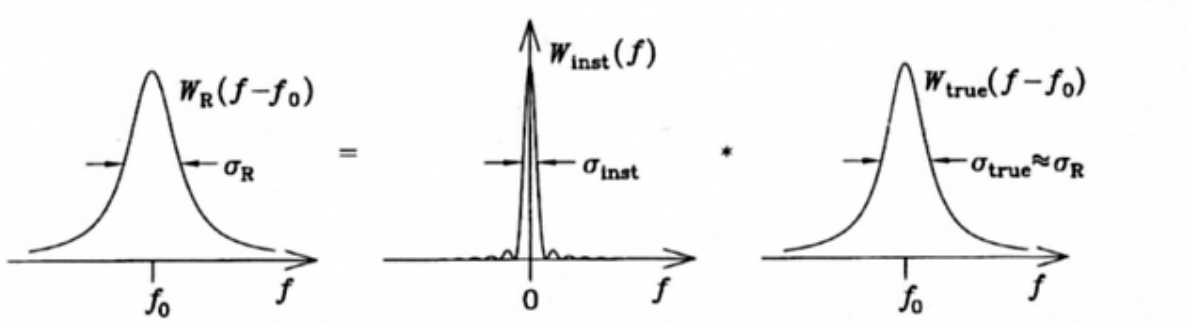

Figure 15: The line shape $W_R(f)$ of a registered high-resolution spectrum $H_R(f)$ is the convolution of the instrumental function of the measurement system $W_{inst}(/)$ and the true line shape *Wtrue(f).*

Figure 16 [16] demonstrates stepwise the procedure of FSD in *f*- and *t*-domains. The behavior of random white noise is shown separately. If we know the line shape $W_R\{ f)$ of the recorded spectrum $H_R(f)$, the only option which may be freely chosen in the FSD procedure is the desired line shape *W(f).* The signal-to-noise ratio of the Fourier self-deconvolved spectrum depends strongly on the shape and the hall-width of *W (f).* This is easy to understand by examining the behavior of noise in Figure 4.3. Consequently the correct choice of *W(f)* is very important in FSD.

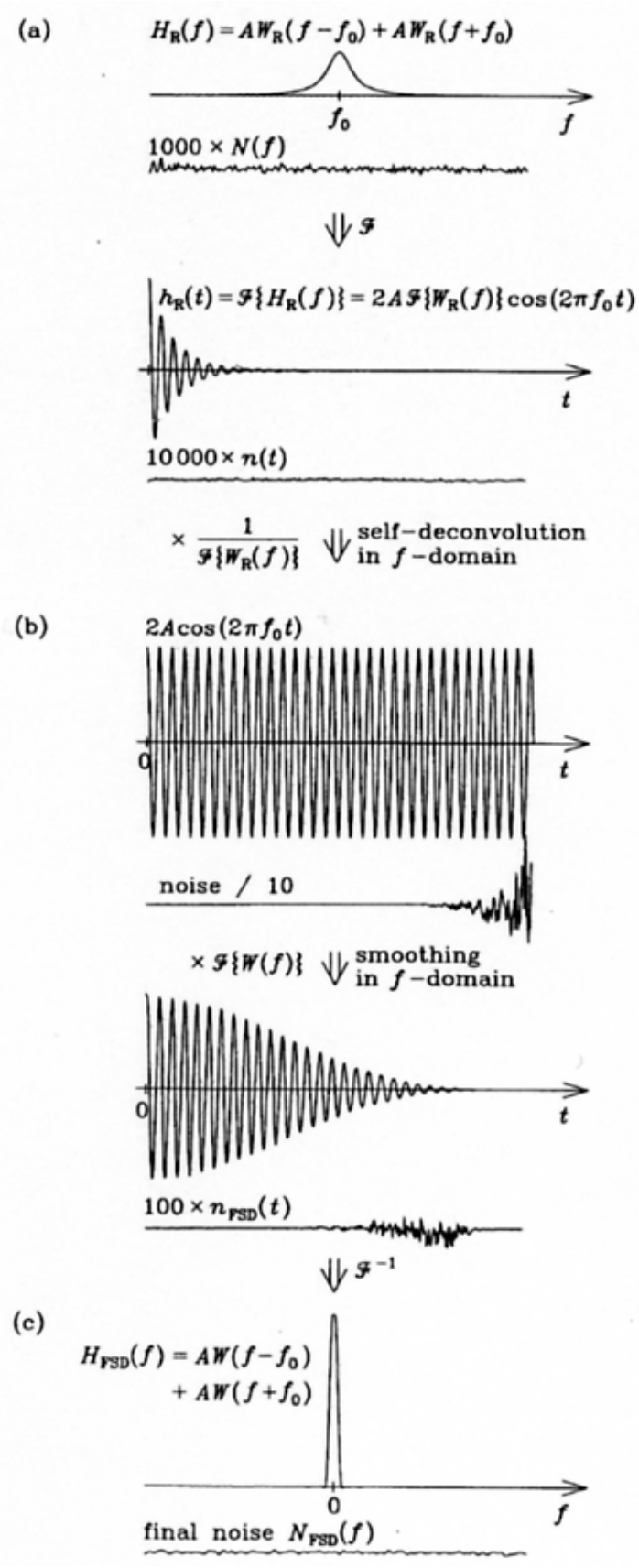

Figure 16: Illustration of the various steps (a) - (c) of the Fourier self-deconvolulion (FSD) procedure.

4.2 Band-separation

Band separation is an application where the usefulness of Fourier self-deconvolution is very obvious. From the Fourier self-deconvolved spectrum we can easily separate a single line, without touching other lines. The desired line may be removed, even if the lines in the original spectrum would overlap. The frequency and the area of the line are preserved. After separation of the desired spectral band, we can restore the line shape information by making an inverse Fourier self- deconvolution. The result is the original line shape, even if the assumed line shape in FSD would not be correct.

Figure 17 shows an FTS simulation which illustrates the band separation procedure. The original spectrum consists of two overlapping Lorentzian lines al the wavenumbers f_1 and f_2, with σR=8 cm^{-1}. The weight function used in FSD is triangular[2], with T =0.8 cm. The original spectrum is first Fourier self-deconvolved by multiplying the corresponding interferogram in the signal domain by $(1-|t| / T)^2 e^{\sigma R \pi |t|}$] and then transforming back to the spectral domain. After that, the line at f_2 is removed. The remaining spectrum, consisting of the line at f_1, is convolved by multiplying the corresponding interferogram by $1 /[(1-|t| / T)^2 e^{\sigma R \pi |t|}]$ and then transforming hack to the spectral domain. The result is the original spectrum with one Lorentzian line [16].

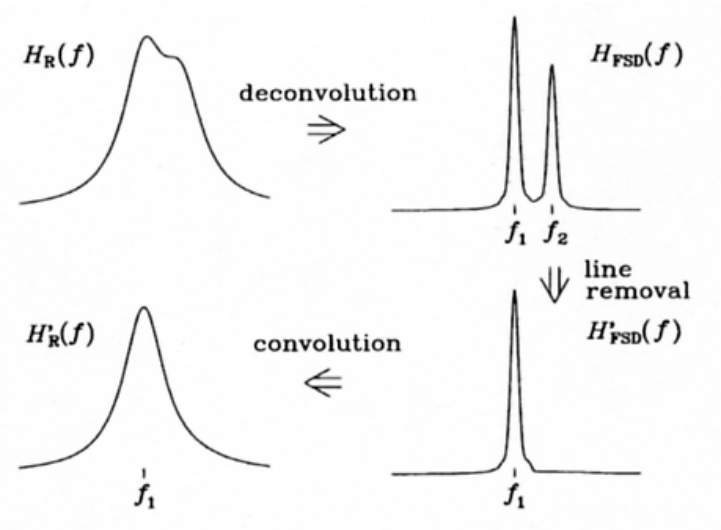

Figure 17. Illustration of the band separation procedure. The original spectrum $H_R(f)$ consists of two Lorentzian lines of the half-width 8 cm^{-1} al the distance 6cm^{-1} from each other. One of the lines is removed from the Fourier self-deconvolved spectrum $H_{FSD}(f)$. The remaining spectrum is Fourier self-deconvolved hack to the spectrum $H'_R(f)$, which differs from the original, became it now consists of only one Lorentzian line.

5. Wavelets

5.1 Introduction to wavelets

The wavelet analysis represents a special type of linear transform of signals and physical data represented by these signals about processes and physical properties of mediums and objects. The basis of the eigenfunctions, on which expansion of signals is spent, possesses many special properties and possibilities. They allow concentrating attention to those or other singularities of analyzed processes which cannot be revealed by means of traditional Fourier and Laplace transforms. Wavelets are the functions of a definite form localized on the axis of arguments (explanatory variables), invariant to shift and linear to operation of scaling (compression/stretching). They form by means of special basis functions which determine their aspect and properties. On localization in temporary and frequency representation wavelets occupy the intermediate position between the harmonic functions localized on frequency, and the function of Dirac localized in time. For the first time this term was used by A.Grossmann and J.Morlet at the analysis of properties of seismic and acoustic signals [17].

The theory of wavelets is not the fundamental physical theory, but it gives the convenient tool for a solution of many practical problems. The basic scope of wavelet transforms is the analysis and processing of signals and functions which are non-stationary in time or inhomogeneous in space, when outcomes of the analysis should contain not only common frequency characteristics of a signal, but also information about the certain local coordinates. In comparison with Fourier series expansion of signals, wavelets are capable with much higher exactitude to represent local singularities of signals. Unlike transforms of Fourier, the wavelet transform of one-dimensional signals ensures two-dimensional result, thus frequency and coordinate are considered as explanatory variables that enables the analysis of signals at once in two spaces. One of the principals of wavelet representation of signals at various levels of decomposition consists in separation of functions of an approximation to a signal on two groups: approximation group, which is rough, with enough slow temporary dynamics of modifications, and detail group, which has local and fast dynamics of modifications on a hum noise of smooth dynamics. It is possible both in temporary, and in frequency areas of wavelet representation of signals. Integral Fourier

transform and Fourier series are the basis of the Fourier analysis. Fourier coefficients received as a result of the transform, give in enough information for simple physical interpretation, and simplicity at all does not belittle importance of the subsequent conclusions about character of an investigated signal. Application of the integral Fourier transform and Fourier series (in evaluations, analytical transforms) is very obvious, all necessary properties and formulas leave by means of only two real-valued functions sin(t), cos(t) (or one complex which is a sine wave [1]

$$\cos(it) = \cos(t) + i\sin(t) \tag{33}$$

5.2 Basic wavelet theory

Wavelet transform is not so good and widely known as Fourier, as it is applied rather recently and is in a stage of active development. We shall briefly describe the bases of wavelet transforms (mainly from the article [18]). $L^2(R)$ is the space of the functions $f(t)$ on the all real axis R (— ∞, ∞). This space has the definition of norm:

$$E_f = \int_0^{2\pi} |f(t)|^2 dt = \sum_{-\infty}^{\infty} |c_n|^2 \tag{34}$$

The spaces $L^2(0.2\pi)$, which is used in expansions of Fourier, and $L^2(R)$ are much different from each other. If we define the space on the all real axis $L^2(R)$, the average value of a function should aspire to zero on ±infinity. The sine wave, in that case, does not belong $L^2(R)$ space, and, hence, the set of sine waves cannot be the basis of this functional space. It is necessary to discover simple enough functions for designing basis of the space $L^2(R)$.

The waves which form the space $L^2(R)$, should aspire to zero at ±∞ and for practical purposes the faster, the better. We shall use well localized solitary waves as the basis functions. They are wavelets.

All Fourier space $R^2(0.2\pi)$, is completely built up by means of only one basis function $\omega(t)$. In the case of wavelets, we will try to build the functional space $L^2(R)$ the same way. That is we use only one wavelet $\psi(t)$. We shall note that it can be a wavelet with one frequency or with a gang of frequencies. Let's first describe discrete transforms.

The task is to cover all real axis R (−∞, ∞) using only one localized function which fast aspires zero. Most simply it can be made, having provided system of shifts or transpositions along an axis. Let for simplicity they will be integer values, i.e. $\psi(t - k)$.

Now we need an analogue of a sine wave frequency. For simplicity we shall note it through degrees of the two: $\psi(2^j t - k)$., here j and k are integers. Thus, by means of discrete scale transforms $(1/2^j)$ and shifts $(k/2^j)$ we can describe all frequencies and cover all axis, having unique basis wavelet $\psi(t)$. [16].

Definition of norm:

$$\|p\|_2 = \langle p, p \rangle^{1/2} \tag{35}$$

$$\langle p, q \rangle = \int_{-\infty}^{\infty} p(t) q^*(t) dt \tag{36}$$

Hence,

$$\|\psi(2^j t - k)\|_2 = 2^{-j/2} \|\psi(t)\|_2, \tag{37}$$

I.e. if a wavelet $\psi \in L^2(R)$ has unit norm, then all wavelets from the set of $\{\psi_{jk}\}$

$$\psi_{jk}(t) = 2^{j/2} \psi(2^j t - k), j, k \in I \tag{38}$$

have also norm 1, i.e. $\| \psi_{jk} \| = \| \psi \|_2 = 1$.

Wavelet $\psi \in L^2$ is called orthogonal if the set $\{\psi_{jk}\}$ defined by the expression (38) represents orthonormal basis of a function space $L^{(R)}$, i.e.

$$\langle \psi_{jk}, \psi_{\ni} \rangle = \delta_{jl} \delta_{km} \tag{39}$$

And each function $f \in L^2(R)$ could be presented in the form of the series

$$f(t) = \sum_{j,k=-\infty}^{\infty} c_{jk} \psi_{jk}(t) \tag{40}$$

A simple example of an orthogonal wavelet is HAAR-wavelet, named so after Haar who had suggested it. This wavelet is defined by the relations

$$\psi^H(t)=\begin{cases}1, & 0\le t<1/2,\\ -1, & 1/2\le t<1,\\ 0, & t<0, t\ge 1.\end{cases} \tag{41}$$

We shall construct basis of a function space $L^2(R)$ by means of continuous scale transforms and transpositions of the wavelet $\psi(t)$ with arbitrary values of basis parameters [18]. We shall use the scale factor a and the parameter of shift b:

$$\psi_{ab}=|a|^{-1/2}\psi\left(\frac{t-b}{a}\right), \quad a,b\in R, \quad \psi\in L^2(R) \tag{42}$$

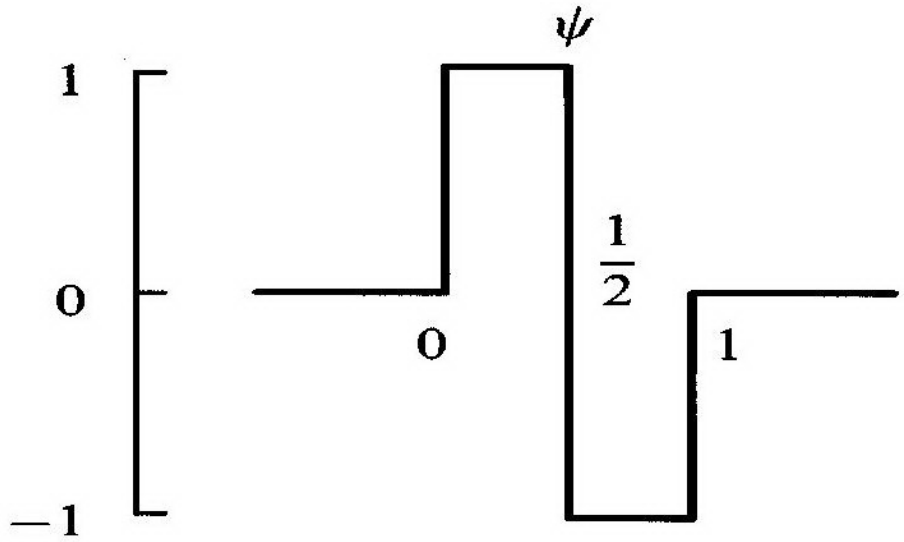

Figure 18. HAAR wavelet.

Now we can write the integral wavelet transform on its basis [19]

$$[W_\psi f](a,b)=|a|^{-1/2}\int_{-\infty}^{\infty} f(t)\psi^*\left(\frac{(t-b)}{a}\right)dt=\int_{-\infty}^{\infty} f(t)\psi^*_{ab}(t)\,dt \tag{43}$$

Let's spend the further analogy to Fourier transform. Coefficients C_{jk} of the wavelet series expansion (30) we can determine through the integral wavelet transform:

$$c_{jk}=[W_\psi f]\left(\frac{1}{2^j},\frac{k}{2^j}\right) \tag{44}$$

So, each function from the space $L^2(R)$ can be determined the sum of scale transforms and shifts of the basis wavelet, i.e. this are a composition of “wavelet waves”.

Use of discrete wavelet transform allows us to lead the proof of many rules of the wavelet theory, connected with completeness and an orthogonality of basis, convergence of series, etc. It is necessary to prove these rules, for example, at compression of the information or in problems of numerical modeling.

Let's consider inverse wavelet transform [19]. The sine wave forms orthonormal basis of the function space $L^2(0.2\pi)$ and problems do not arise with inverse transform of Fourier. But in the wavelet transforms the basis $L^2(R)$ is not always orthonormal. It is defined by a choice basis wavelet, and a mode of construction of the basis (values of basis parameters *a*, b). However strict proofs of completeness and orthogonality are complicated. Besides for practical purposes it is enough to have "approximate" orthogonality of a system of expansion functions i.e. that is enough, that it is "almost the basis".

Let's write out inverse transform for those two cases that are described above: for the basis (38) supposing expansions and shifts, and the basis (42) constructed at arbitrary values (*a, b*).

At the basis parameters (*a, b*), a, $b \in R$ inverse wavelet transform is written by means of the same basis, as the direct [18]:

$$f(t)=C_{\psi}^{-1}\int\int[W_{\psi}f](a,b)\psi_{ab}(t)\frac{da\,db}{a^2}, \tag{45}$$

C_{ψ} is the normalizing coefficient (similar to the coefficient which normalizes Fourier transform):

$$C_{\psi}=\int_{-\infty}^{\infty}|\hat{\psi}(\omega)|^2|\omega|^{-1}d\omega<\infty \tag{46}$$

The condition of finiteness of the constant C limits the class of functions which can be used as a wavelet basis. In particular, it is obvious, that the Fourier imager should be equal to zero at the origin of coordinates and, hence, it should be equal to zero at least at zero moment: $\int_{-\infty}^{\infty}\psi(t)dt=0.$

More often in applications are enough reviewing only positive frequencies, i.e. $a>0$. Wavelet, accordingly, should satisfy to the condition

$$C_{\psi}=2\int_{-\infty}^{\infty}|\hat{\psi}(\omega)|^2|\omega|^{-1}d\omega=2\int_{-\infty}^{\infty}|\hat{\psi}(-\omega)|^2|\omega|^{-1}d\omega<\infty \tag{47}$$

In case of discrete wavelet transform the steady basis is defined as follows.

Function $\psi \in L^2(R)$ is called R-function if the basis $\{\psi_{jk}\}$, defined by expression (38), is the basis of Rises in the sense that there are two constants A and B, for which the relation

$$A\|\{c_{jk}\}\|_2^2 \le \left\| \sum_{j=-\infty}^{\infty} \sum_{k=-\infty}^{\infty} C_{jk} \psi_{jk} \right\|_2^2 \le B\|\{\} c_{jk}\|_2^2 \tag{48}$$

is true at any sequences $\{C_{jk}\}$:

$$\|\{c_{jk}\}\|_2^2 \le \sum_{j=-\infty}^{\infty} \sum_{k=-\infty}^{\infty} |C_{jk}|^2 < \infty. \tag{49}$$

For any R-function there is a basis $\{\psi^{jk}\}$, which is "double" of basis $\{\psi^{j}_{k}\}$, by means of which it is possible to construct the reconstruction expression

$$f(t) = \sum_{j,k=-\infty}^{\infty} \langle f, \psi_{jk} \rangle \psi^{jk}(t) \tag{50}$$

If ψ is the orthogonal wavelet and $\{\psi_{jk}\}$ is the orthonormal basis then $\{\psi^{jk}\}$ and $\{\psi_{jk}\}$ coincide and the formula is formula of inverse transform. If ψ is not orthogonal wavelet, but is two-place or conjugate R-wavelet, it has the double ψ by means of whom the double of a set $\{\psi_{jk}\}$ is constructed similarly to the basis [18]:

$$\psi^{jk} = \psi^{*}_{jk} = 2^{j/2} \psi(2^{j}t - k), \; j, k \in I. \tag{51}$$

5.3 Wavelet analysis applied to removing of a spectroscopic background

Spectroscopic background can be divided into two types: constant and varying. In the first case background correction does not represent difficulties since the background remains constant at various spectral measurements. However, in the second case, when spectroscopic background is not constant at various measurements, correction is a rather difficult task, especially if it should be made automatically.

Further the so-called algorithm of a "wavelet prism" (which is explained in the article [20]) is described. According to the theory of wavelets, the signal in the space $L^2(R)$ has unique wavelet representation, if certain conditions are met. The discrete signal f_i, for example, can be presented

$$f_i = g_{i-1} + \ldots + g_{i-l} + f_{i-l} \tag{51}$$

Where f_{i-l} is the approximation component, which frequency is no larger, than 2_{i-l}. This component is orthogonal to the detail components x_j at various levels j ($j= i-1,\ldots , i-l$). These detail components in turn are orthogonal among themselves and their frequencies are in a range from 2^{j+1} up to 2^j. Generally undesirable spectroscopic background is a low-frequency component of the signal. Thus, for a solution of the problem of background correction it is possible to use wavelet decomposition. It does not depend on the type of a background (constant or varying).

On the basis of the fast wavelet transform algorithm (Mallat algorithm [19]), decomposition can be made by means of the linear mathematical operations using scaling function and wavelet orthogonal filters: a low pass filter H and a high pass filter *G*.

We can write for the first linear transform:

$$\begin{cases} c^1_{i-1} = Hc^0_i \\ d^1_{i-1} = Gc^0_i \end{cases} \tag{52}$$

Thus, for the j^{th} transform we have

$$\begin{cases} c^{j+1} = Hc^j \\ d^{j+1} = Gc^j \\ j = 0,1,\ldots,l. \end{cases} \tag{53}$$

This decomposition can be presented as

$$\begin{array}{ccccccccc} c^0 & \rightarrow & c^1 & \rightarrow & c^2 & \rightarrow & \ldots & c^{l-1} & \rightarrow & c^l \\ & \searrow & & \searrow & & \searrow & & \searrow & \\ & & d^1 & & d^2 & & d^3 & \ldots & d^l \end{array} \tag{54}$$

Low-frequency and high-frequency filters define approximation and detail coefficients. High-frequency coefficients have high resolution whereas low-frequency coefficients have low resolution. However, these two types do not give the information about the time resolution of the spectrum for deriving the information about spectroscopic background. The basic difficulty here consists in definition of a level of wavelet decomposition on which spectroscopic background is observed which is necessary for its removing [20].

Generally reconstruction of an original spectroscopic signal can be lead by means of inverse linear wavelet transform:

$$c^j = H^T c^{j+1} + G^T d^{j+1}, \quad j = 0,1,\dots,l \tag{55}$$

Transform can be presented also as:

$$\begin{array}{ccccccccc} c^l & \rightarrow & c^{l-1} & \rightarrow & \dots & c^2 & \rightarrow & c^1 & \rightarrow & c^0 \\ & \nwarrow & & \nearrow & & & \nwarrow & & \nearrow & \\ d^1 & & d^{l-1} & & \dots & d^2 & & d^1 & & \end{array} \tag{56}$$

Wavelet inverse transform is a linear transformation; therefore it can be presented as

the sum of terms:

$$f\,(=c^0) \approx g_1 + g_2 + \dots + g_l + f_l \tag{57}$$

Where:

$$\begin{aligned} g_1 &= G^T d^1 \\ g_2 &= H^T G^T d^2 \\ &\vdots \\ g_l &= \underbrace{H^T H^T \dots H^T}_{l-1} G^T d^l \\ f_l &= \underbrace{H^T H^T \dots H^T}_{l} c^l \end{aligned} \tag{58}$$

Approximation (f_1) and detail ($g^l, \dots, g^2, g^1$) components are reconstructed directly from wavelet coefficients ($c^l, d^l, \dots, d^2, d^1$). These components are orthogonal among themselves, create the contribution of various ranges of frequencies to a signal and have same resolution as the original signal. As shown in a Figure 7, the described wavelet transform splits a signal like a prism splits light waves. Such method is called method of “wavelet prism”.

It is visible in the figure that the probable spectroscopic background can be found in the lowest frequencies (such as f_{10}). Noise components are found at high-frequency components (such as g_1,g_2).

Thus, the following two conclusions were made in the article [20]:

• The spectroscopic background is the spectral component arranged in low frequencies of wavelet decomposition (f_b), whereas the useful signal is located in middle frequencies (g_s). Noise is the third component of a spectrum, which is usually observed on the higher frequencies (g_n).

• Background, useful and noise components of a signal are not superimposed among themselves and submit to a rule of additive

$$f = g_n + g_s + f_b \tag{59}$$

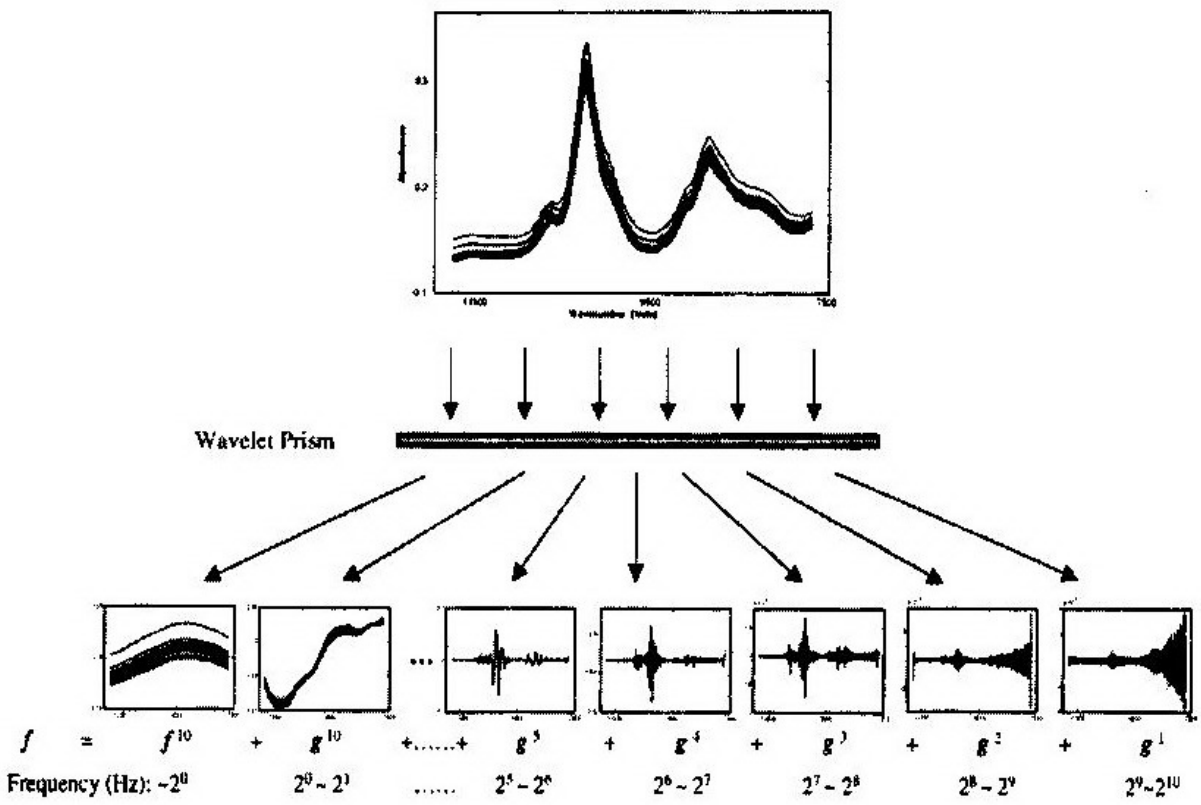

Figure 19. “Wavelet prism” principle [18]

Thus, there is a possibility to eliminate the last item in the expression (59), as it will be elimination of a spectroscopic background.

6. Experimental section

6.1 CARS spectrometer

For further researching CARS spectrometer is needed. Also some specters are necessary for continuation of work, to use it as basic data for the analysis.

The experimental setup for CARS measurement consists of: two lasers “Laser” which generates 10ps impulses (bandwidth 1.5 cm^{-1}full width at half maximum (FWHM) on a wave length 710nmis overlapped in time and space, with a “Stokes” laser which generates 80fs. The Stokes laser is tunable between 750-900nm, corresponding to a vibration range of ~750-3500 cm^{-1}Typical laser powers are 75 mW and 105 mW for the pump and Stokes laser respectively. They are focused by an objective of the microscope O1 on an investigated sample. Scattered CARS signal is collected in the forward direction by the second objective O2 and transited through the holographic filter F1 and the short wave-filter F2. The generated anti-Stokes signal spectrally resolved on a spectrometer with CCD sensors and an effective spectral resolution of ~5 cm^{-1}. The schematic diagram of CARS spectrometer is represented in a figure 20.

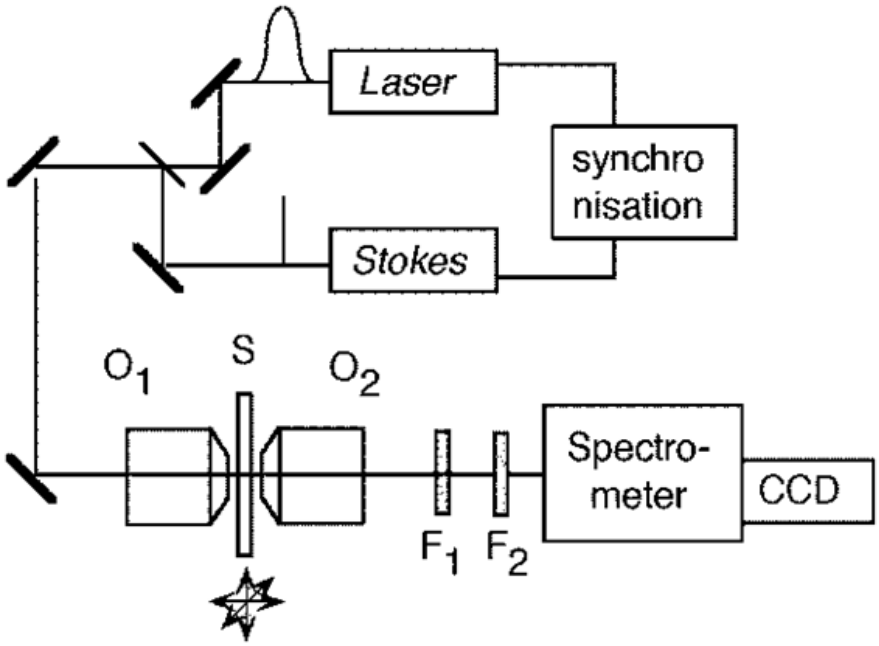

Figure 20. The schematic diagram of CARS spectrometer

6.2. Experimental data

In this part is presented the test spectra for the analysis.

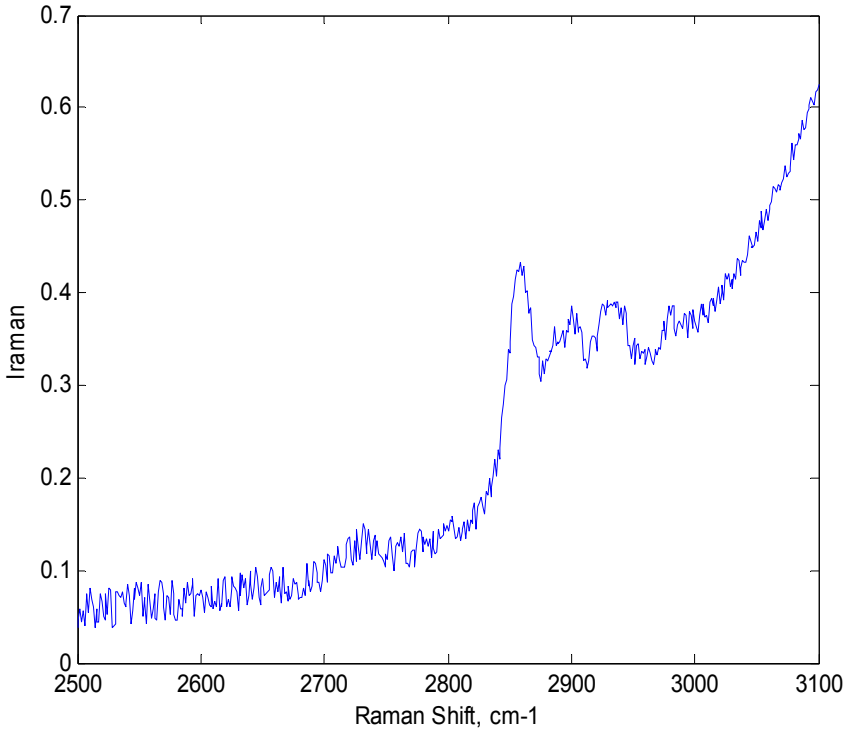

Figure 21. True phase spectrum with large non-constant background connected to a multiplex CARS measurement

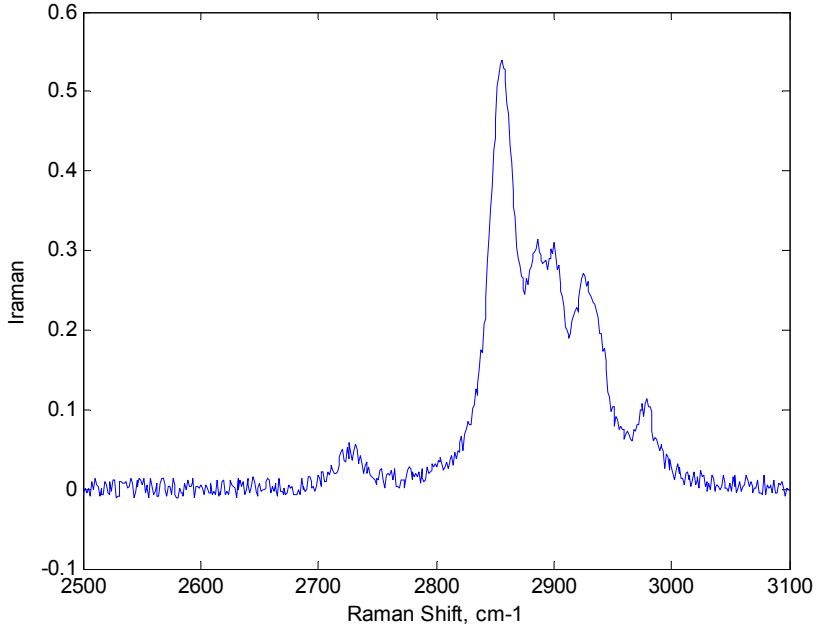

Figure 22. Imaginary part of the spectrum with a constant background of the spectra connected to a multiplex CARS measurement

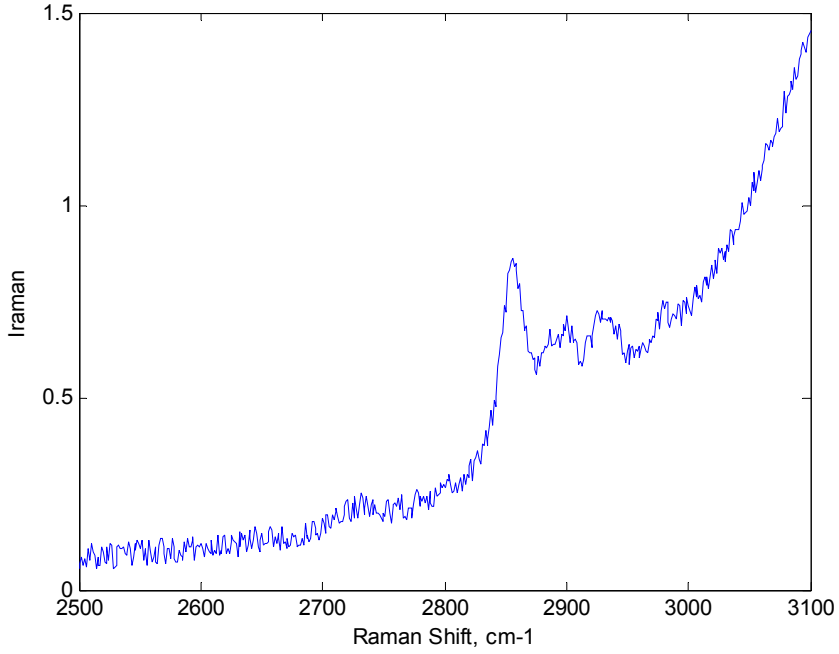

Figure 22 . Imaginary part of the spectrum with large non-constant background of the spectra connected to a multiplex CARS measurement

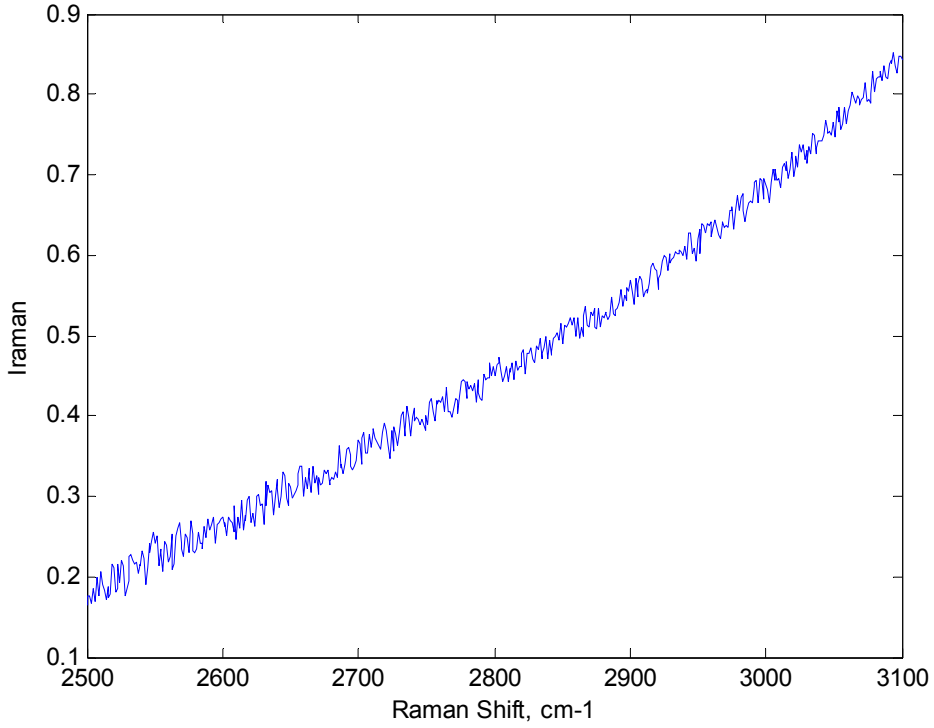

Figure 23. A phase term showing the

slowly varying background of spectra connected to a multiplex CARS measurement

6. Description of the algorithm.

6.1. Basic components of the algorithm.

The main idea of the Thesis is to learn to do the FSD to ME-phase spectra. However, firstly we applied FSD transformations to the imaginary part of the simulation spectra without background. But we need to apply FSD to ME-phase and to be able to get rid of the background from it. Some cases this background can be removed already by wavelet decomposition (WD), but in particular in those cases where the spectrum is very congested (i.e. there are many closely lying spectral lines such that single spectral lines are not visible) the WD won't work well. Then, if the spectral lines could be made narrow enough (by FSD, or by FSD + linear prediction), there is a good change that WD would work good enough in removing the background from the ME phase. This means, furthermore, that we'll are able find the true phase function from the ME-phase. Of course, if the original "true" phase line shape is wanted, we need to do an "inverted FSD" in the final step of the procedure, to make the spectral lines as broad as they were originally.

But before FSD transformations it is necessary to make wavelet decomposition to the phase spectrum to get rid of noise.

So, the main steps in FSD are:

1) Compute the FFT (preferably by cosine-FFT) of the spectrum. This will give discrete data of a sum of decaying cosine waves.

2) Choose a line-shape function, for example, a Lorentzian line-shape would be the most natural choice:

$$L(\omega) = \Gamma^2/(\omega^2 + \Gamma^2) \tag{60}$$

3) Fourier transform the line-shape function, in case of above L(ω), this will give an exponential function:

$$y(m) = A \exp[-a(m-1)],\ m=1,2,3,..,N \tag{61}$$

4) Normalize y(m): y'(m)=y(m)/A

5) Divide the FFT of the spectrum, which gives depending on the chosen line width Γ, either (a) non-decaying cosine waves (i.e. cosine waves with constant amplitude), (b) cosine waves with increasing amplitude, or (c) slower decaying cosine waves as the original.

In case of (a) the selected value for Γ is exactly correct; in (b) Γ is too small, and in (c) Γ is too large. (a) and (c) are OK in FSD, the (b) is not.

6) After smoothing the non-decaying cosine waves take an inverse FFT of them.

7) Apply wavelet decomposition to remove background.

6.2. Realization the developed algorithm.

1. All computations on spectroscopic noise removal were made in the mathematical software MATLAB. Applying wavelet transformations for de-noising as noise reduces significantly the amount of line width narrowing. To perform WT decomposition we need to decide two things: (1) the decomposition level (n) and (2) the wavelet type. For example, mainly used a Daubechies wavelet db8 with a decomposition level of n=7 or n=8. Also the Symlet wavelets work well sym8. There were used Daubechies wavelets with scale parameter n= 8.

2. Use of the multilevel one dimensional discrete fast wavelet transform to the calculated phase function $\psi(\upsilon)$. Decomposition of this function is calculated up to some level *l* (which is usually equal to 6 - 8). The result is presented as number of approximation and detail coefficients. The function of multilevel wavelet transform from MATLAB *xd*=*wden* (*x, TPTR, SORH, SCAL, N, wname*) was used, where *x* is a signal, *TPTR* is the line which determine the threshold (*sqtwolog), SORH* the selection of the kind of the threshold soft or hard (*soft*), *SCAL* is the option that select multiplicative threshold of the over scaled coefficients. If the noise is more than [0.1] the threshold must be over scaled by the level of the noise ('*sln*'), *N* is the necessary level of decomposition (equal 8), *wname* is the wavelet-basis of decomposition ("db10").

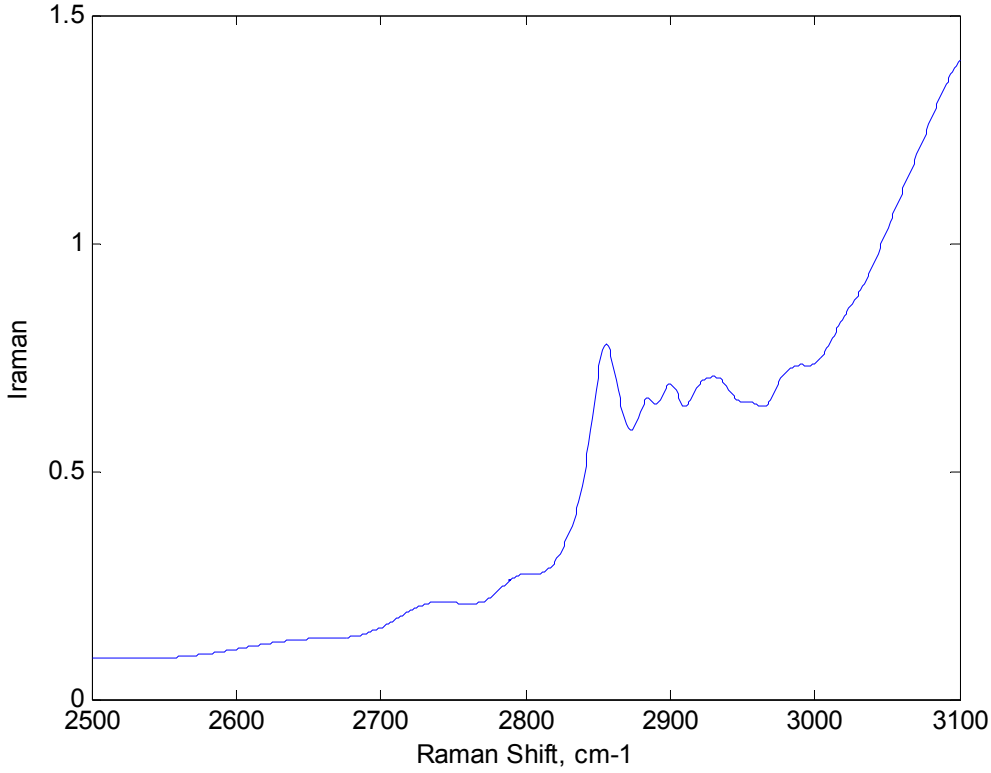

Figure 24. Estimated imaginary part of the spectrum without noise

On the basis of the analysis, we make a decision, whether the signal is satisfactory for the further analysis of components containing in a sample. If it is not satisfactory, we decrease or increase the decomposition level *l* and repeat step 2. If all decomposition levels were tested and are not acceptable, chose different scale parameter of the wavelet and repeat step 1.

3. The tested algorithm on the imaginary part we apply FSD to the de-noised imaginary part. We took a cosine FFT of the original data (y(1), ..., y(N)). However it is possible to use the normal exponential Fourier transform. In this case in the beginning we should add "a mirror image" to the data, i.e., if the data is a set of N discrete values:

$$y(1),y(2),..y\ (N), \tag{62}$$

we need to replace this set of data with the new set of the values as:

$$y(1),y(2),..y(N),\ y(N),y(N-1),y(N-2),...y(1) \tag{63}$$

And will get a complex values Fourier-transform.

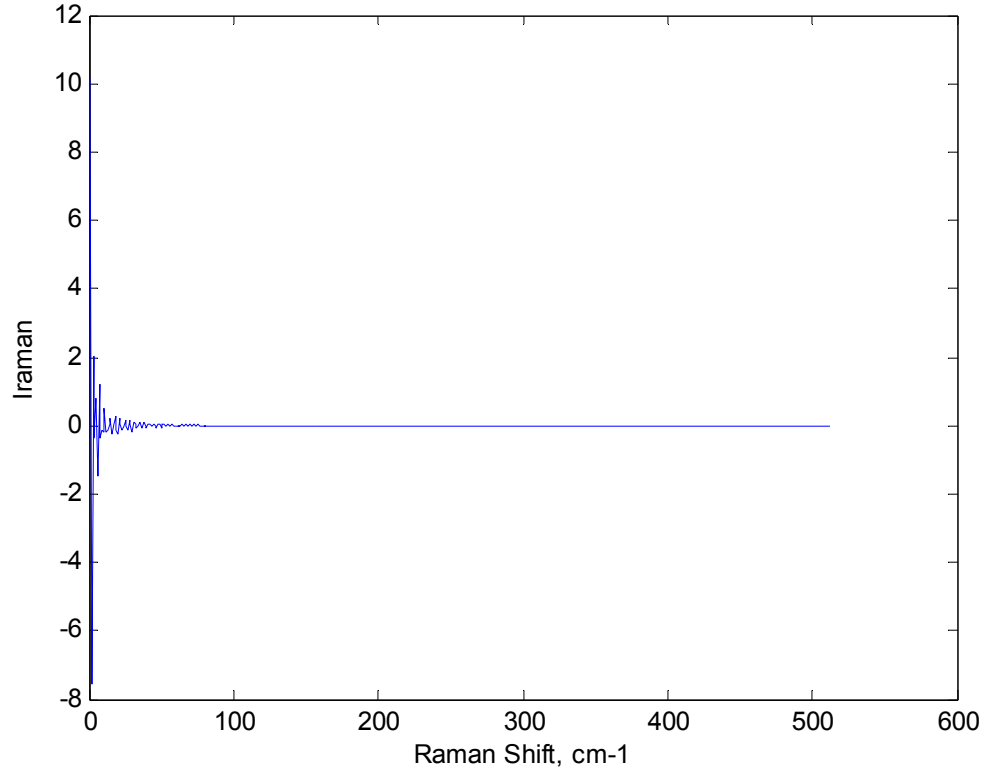

Figure 25. Fourier transform (FFT) of the spectrum

4. A chosen line-shape function is $L(\omega) = \Gamma^2/(\omega^2 + \Gamma^2)$. Fourier transform the line-shape function, in case of L(ω), will give an exponential function:

$$g'(t) = exp\,(2\,p\,\Gamma t), \tag{64}$$

where the discrete time, t(n), used in computations can be defined here as follows:

$$t(n) = (n - 1)/(2\Delta\omega) \tag{65}$$

where $\Delta\omega$ is the length of the spectrum range: $\Delta\omega = \omega_{max} - \omega_{min}$, n is the index: $n = 1, 2, 3, \ldots, N$; and where N is the number of the samples.

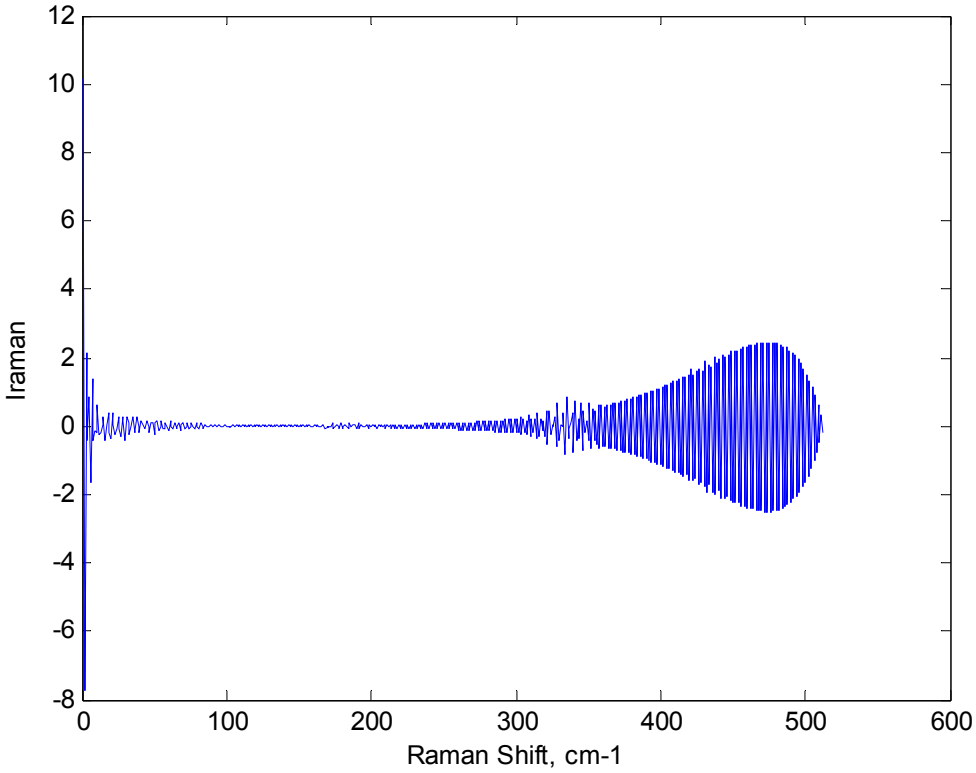

Figure 26. Spectrum W'(t). Multiplication the FFT of the imaginary part by a line shape Function

5. Divide the FFT of the spectrum, which gives (a) non-decaying cosine waves (i.e. cosine waves with constant amplitude), depending on the chosen line width Γ. The other way it is possible to get (b) cosine waves with increasing amplitude or (c) slower decaying cosine waves as the original. In case of (a) the selected value of Γ is absolutely correct; in (b) is too small, and in (c) is too large. In Figure (26) is presented the (a) case.

Now the FSD spectrum needs to be smoothed; smoothing was done with a Bessel function:

$J(t) = (1 - (t/T)^2)^2$.

Before smoothing the tail of the FSD was set to zero after N=160 as to avoid the additional background.

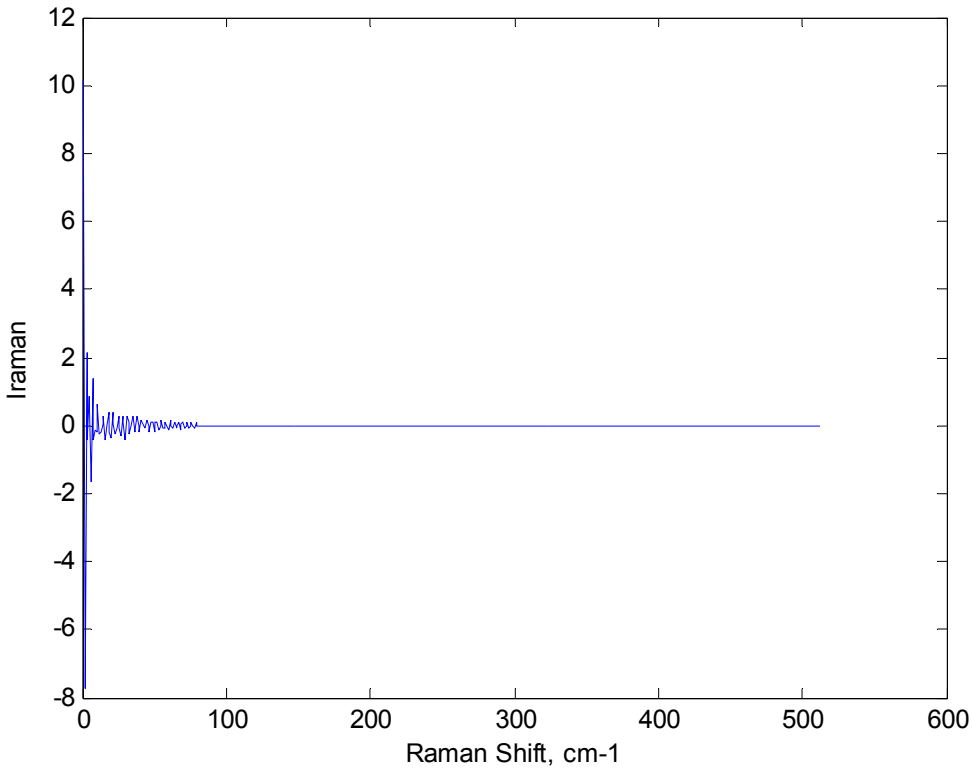

Figure 27. Multiplication of the Spectrum W'(t) with the apodization function $A(t) = A(n) = (1-(n-1)^2/(N-1)^2)^2$

6. Getting us a new spectrum by inverse transform of the latter in the final step of the procedure to get the original "true" phase line shape, to make the spectral lines as broad as they were originally.

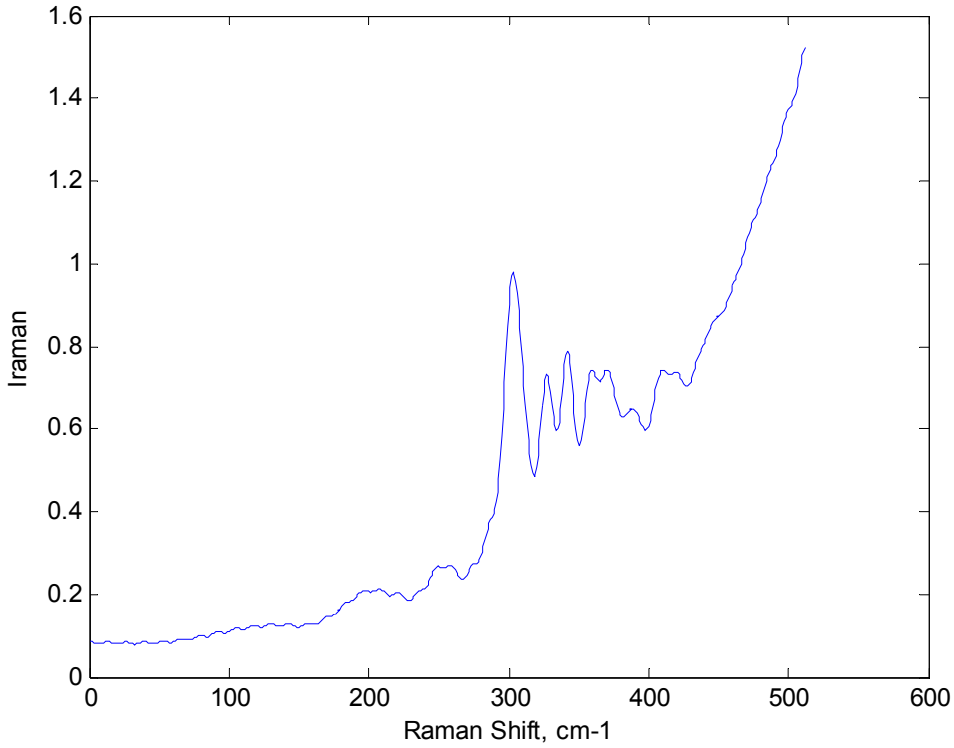

Figure 28. De-noised spectrum with reduced widths of lines

7. Finally, apply WT again to get rid of the background. We upload the line-narrowed de-noised (Figure 28). The function of multilevel wavelet transform from MATLAB *[C ,L]=wavedec(y , l ,wwl)* was used, where *y* is the initial function (phase function), *l* is the necessary level of decomposition (equal 6), wwl is the wavelet-basis of decomposition ("db10"). Calculated vectors C and L contain a set of approximation and detail coefficients which will be used for inverse decomposition of a signal.

We restore a signal, using only detail coefficients (on one branch of coefficients on a signal), and also the l^{ath} branch of approximation coefficients. The function *xn=wrcoef (type ,C , L ,wwl , n)* was used, where *type=' a '* for reconstruction on a branch of approximation coefficients and *type=' d'* for reconstruction on a branch of detail coefficients, *n* is the level of decomposition (from 1 up to 8 for detail coefficients and 8 for approximation coefficients) is used. Thus we obtain nine functions, representing "prismatic" decomposition on wavelet frequencies.

Nine signals are presented in Figure 29. The first graph reflects the contribution of the highest frequencies, and last reflects the lowest. The spectroscopic background of a signal places on the lowest frequencies. Here the background is at the last graph in the figure. Now it is enough to

restore the initial signal, using only eight branches of detail coefficients, in other words, to sum and then to normalize functions at n equal from 1 up to 8. This signal should not contain the spectroscopic background. The result of the low frequency removal from the imaginary part is presented in Figure 30.

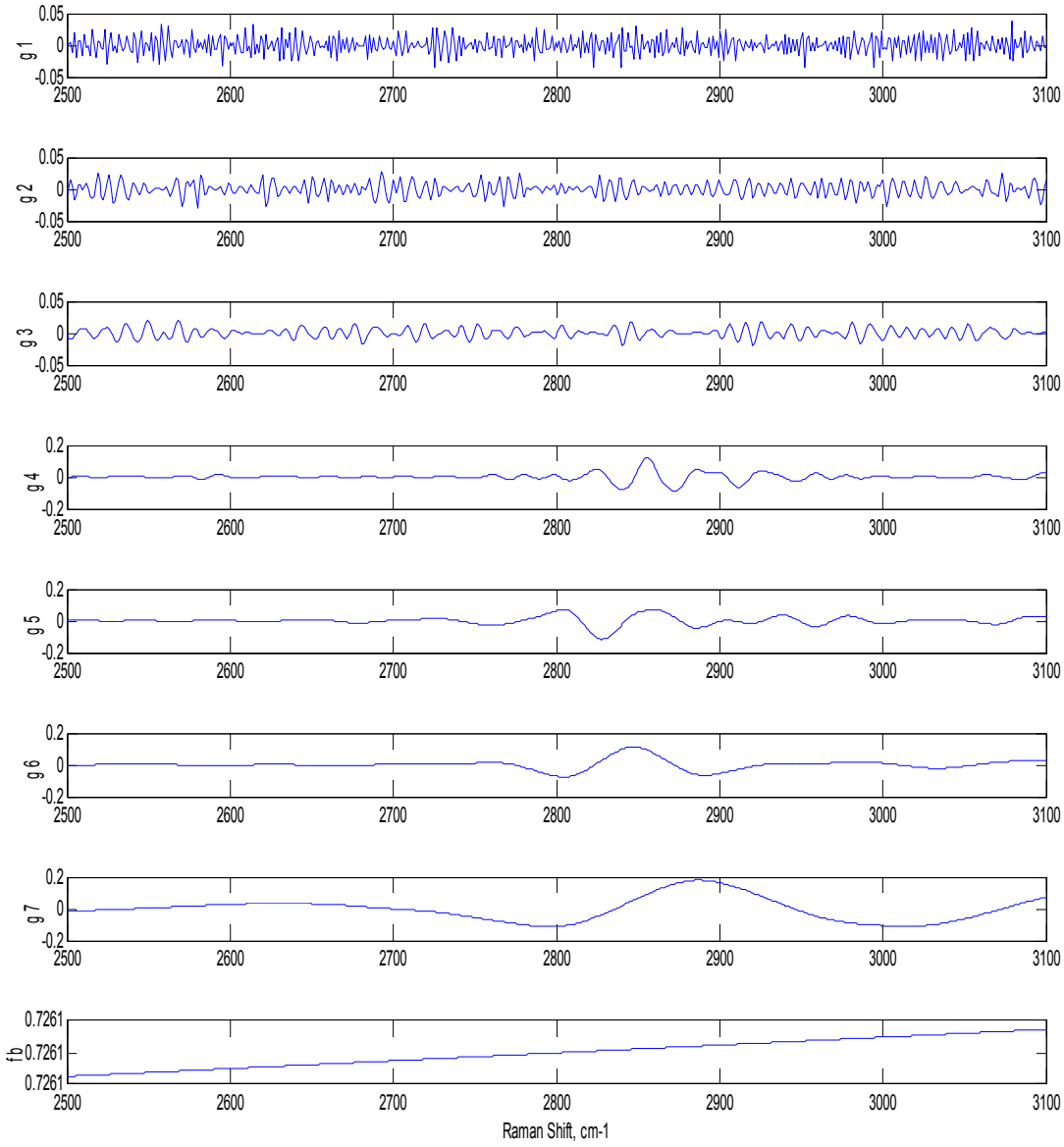

Figure 29. Realization a method of a “wavelet prism” for the spectrum

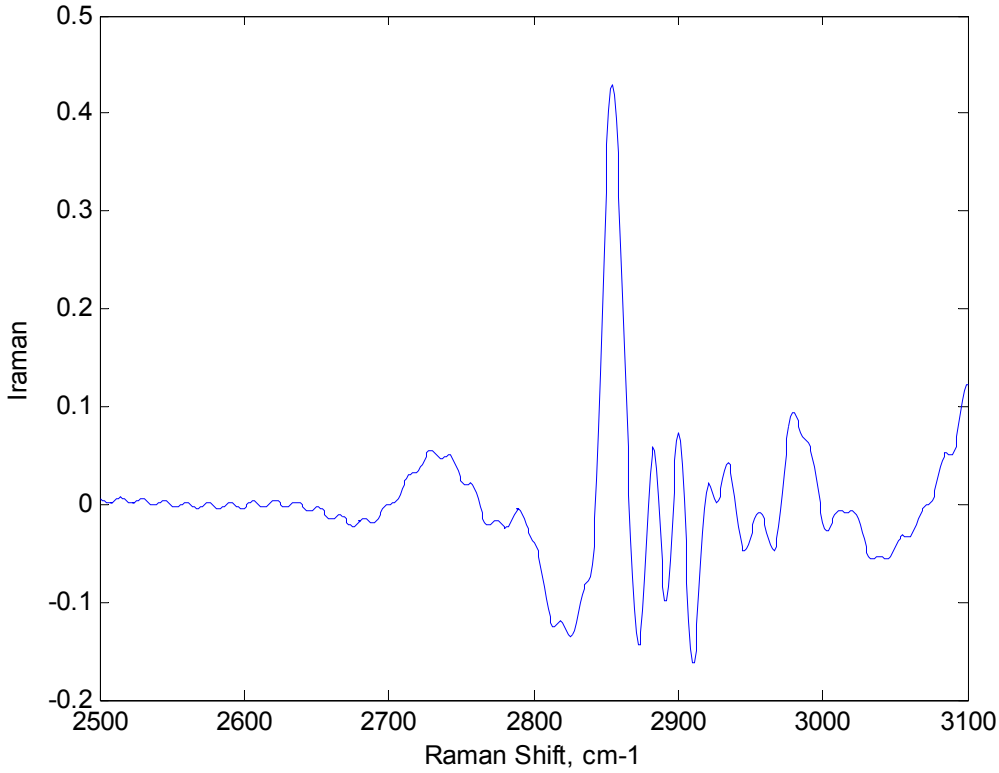

Figure 30. Estimated imaginary part without background

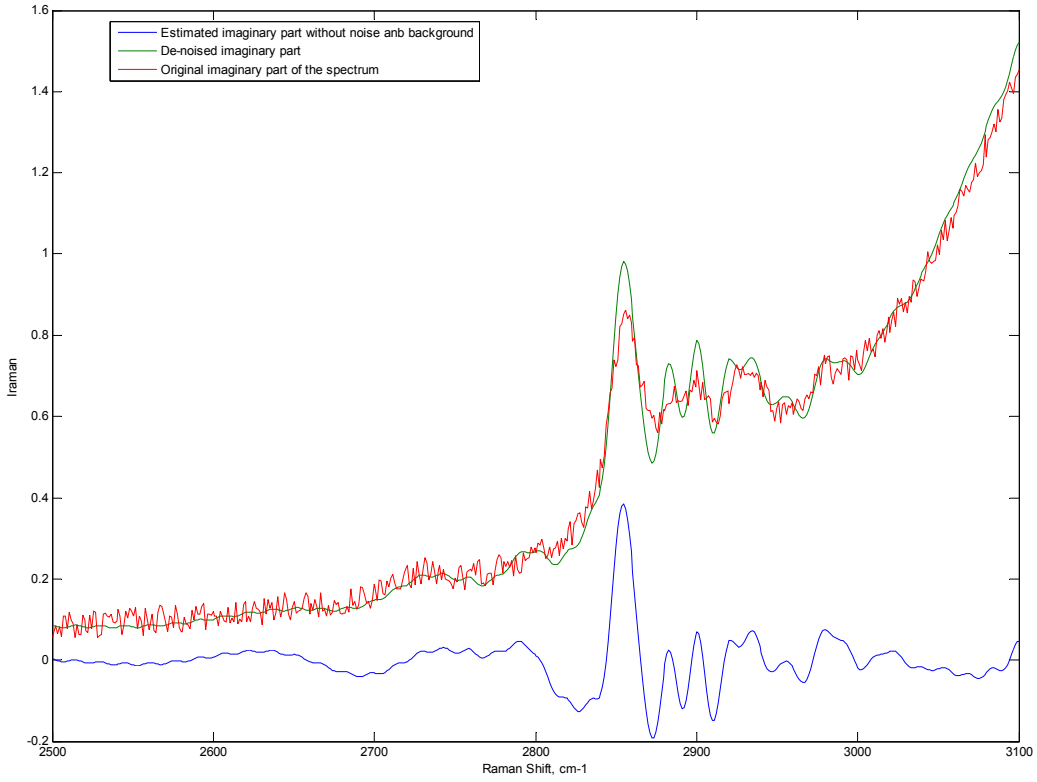

Figure 31. Imaginary part without noise and removed background

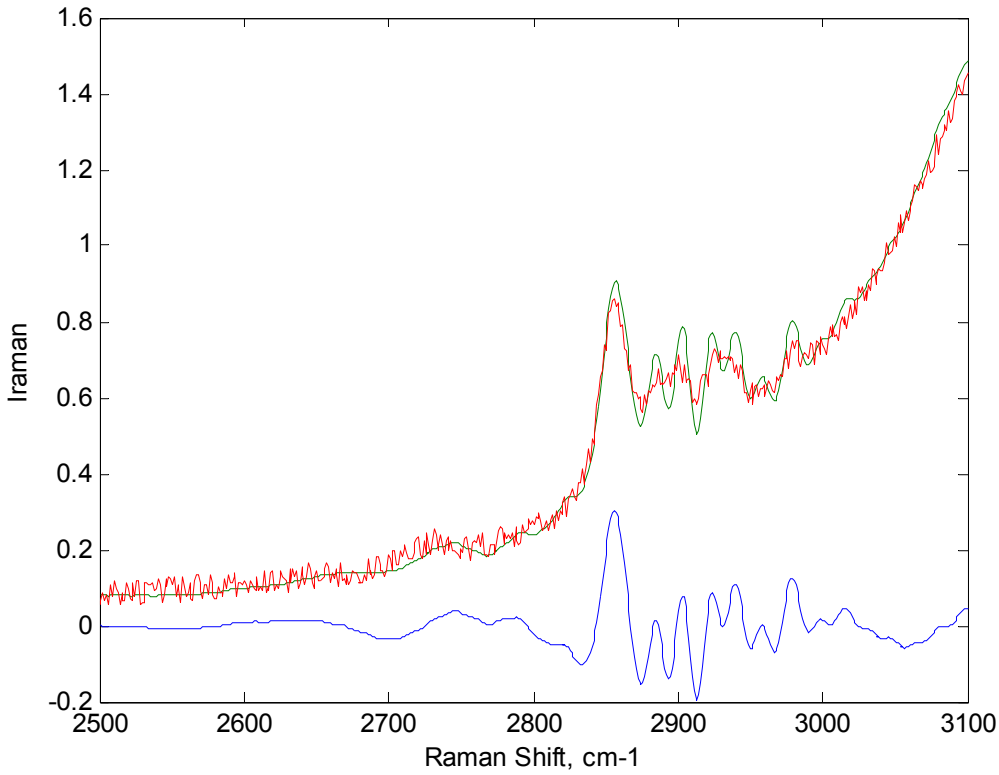

Figure 32. Estimated Raman Imaginary part without noise and removed background with another wavelets perametres.

Figure 32 shows spectrum with better band separation and the noise has lower level. The scale parameter of the Daubechies wavelet for noise removing has been taken equal 15 ("*db15*"), the decomposition level has been also taken *l* = 8.

Now it is possible to test the algorithm on the ME-phase spectrum Figure 23. After we apply absolutely the same steps we get Figure 31 which demonstrate us original ME-phase, de-noised and spectrum without background.

7. Conclusions

In the presented Thesis the main idea was to combine the wavelets decomposition and Fourier Transformation for reducing the widths of spectral lines. The input data for the algorithm is a CARS spectrum of intensity, measured by a CARS spectrometer. And the output data is the corresponding calculated imaginary part and ME-phase based only on information from CARS measurements.

Accordantly to this procedure, we first compared the method of wavelets for removing the noise from the signal. After check of set of wavelets with various scales of functions it has been decided, that Daubechies wavelet with the scale of function 8 has the best characteristics for the task. Further for wavelet decomposition of a signal was chosen a level of decomposition, i.e. how many times wavelet transforms will be made. The number of decomposition coefficients depends on it, we accepted a level equal $l = 8$. Figure 24 shows the result.

Then applied the method of Fourier Self-Deconvolution proved its well established procedure for spectral line –narrowing. Despite the fact that it is a noisy method we could get result with a small level of noise because of make use of wavelets.

Removal of a spectroscopic background is more difficult task. Earlier methods used approximation, being based on the fact, that vibration resonances are narrow components on a large background. The method of the wavelet analysis of spectra with the purpose of removal of a low-frequency background and high-frequency noise from spectra was suggested. Estimated imaginary part without background is shown on Figure 30 with parameters of Daubechies wavelet with a scale of function 10 and a level $l = 8$ was accepted

It was noticed, that the wavelet method in compare with FSD cannot sometimes provide the same accuracy as manual fitting of line-narrowing procedure. The result can be improved by selecting a different wavelet. The main advantage is that the algorithm can have easy realization in a computer program. As all the calculations were made in MATLAB, the programme can be to rewrite easily to a program which can provide additional specifications to a new spectrum.

8. References.

1. G. R. Holtom, B. D. Thrall, B. Chin and D. Colson, Traffic 2, 781-788 (2001).

2. G. J. Puppels, F. F. M. de Mul, C. Otto, J. Greve, M. Robert-Nicoud, D. J. Arndt-Jovin and T. M. Jovin, Nature 347, 301-303 (1990).

3. H. van Manen, Y. M. Kraan, D. Roos and C. Otto, Proc. Natl. Acad. Sci. USA 102(29), 10159-10164 (2005).

4. X. Nan, J. X. Cheng and X. S. Xie, J. Lipid Res. 44(11), 2202-2208 (2003). P. Kennedy, J. Sutcliffe and J. X. Cheng, Langmuir 21(14), 6478-6486 (2005).

5. L. Evans, E. O. Potma, M. Puoris'haag, D. Cote, C. P. Lin and X. S. Xie, Proc. Natl. Acad. Sci. USA 102(46), 16807-16812 (2005).

6. J. Cheng, A. Volkmer, L. D. Book and X. S. Xie, J. Phys. Chem. B 106(34), 8493 -8498 (2002).

7. M. Müller and J. M. Schins, J. Phys. Chem. B 106(14), 3715-3723 (2002)

8. G. R. Holtom, B. D. Thrall, B. Chin, and D. Colson, "Achieving molecular selectivity in imaging using multiphoton Raman spectroscopy techniques," Traffic 2, 781-788 (2001).

9. J. X. Cheng and X. S. Xie, "Coherent Anti-Stokes Raman Scattering Microscopy: Instrumentation, Theory, and Applications," J. Phys. Chem. B 108, 827-840 (2004).

10. A. Volkmer, "Vibrational imaging and microspectroscopies based on coherent anti-Stokes Raman scattering microscopy," J. Phys. D: Appl. Phys. 38, R59-R81 (2005).

11. G. J. Puppels, F. F. M. de Mul, C. Otto, J. Greve, M. Robert-Nicoud, D. J. Arndt-Jovin, and T. M. Jovin, "Studying single living cells and chromosomes by confocal Raman microspectroscopy," Nature 347, 301-303 (1990).

12. H. van Manen, Y. M. Kraan, D. Roos, and C. Otto, "Single-cell Raman and fluorescence microscopy reveal the association of lipid bodies with phagosomes in leukocytes," Proc. Natl. Acad. Sci. USA 102, 10159-10164 (2005).

13. N. B. Delone, “Nelinejnaja optika” (“Nonlinear optics”, in Russian), Soros Educational Journal, №3, 94-99 (1997)

14. W. Hubschmid, R. Bombach, “Laser spectroscopy in combustion research”, Introduction to numerical methods in combustion research, Ercoftac summerschool, 4.1-4.12 (2002)

15. N. I. Korotneev, “Interferencionnye javlenija v kogerentnoj aktivnoj spektroskopii rassejanija i poglowenija sveta: golograficheskaja mnogomernaja spektroskopija” (“Interference effects in the coherent active spectroscopy of scattering and absorption of light: the holographic multivariate spectroscopy”, in Russian), Advances in Physical Sciences, vol. 152, no.3, 493-518 (1987)

16. J. Kauppinen and J. Partanen, Fourier Transforms in Spectroscopy (Wiley, New York, 2001)ISBN 3-527-40289-6.

17. A. V. Davydov, “Vejvlety. Vejvletnyj analiz signalov” (“Wavelets, wavelet-analysis of signals”, in Russian), http://prodav.narod.ru/wavelet/index.html (2007)

18. N. M. Astafieva, “Vejvlet-analiz: osnovy teorii i primery primenenija” (“Wavelet analisys: the basics of theory and examples of application”, in Russian), Advances in Physical Sciences, Vol. 166, №11, 1145-1170 (1996)

19. N.K. Smolentsev, “Osnovy teorii vejvletov. Vejvlety v MATLAB.” (“Basics of the wavelet theory. Wavelets in MATLAB”, in Russian), DMK-Press (2005)

20. H. W. Tan, S. D. Brown, “Wavelet analysis applied to removing non-constant, varying spectroscopic background in multivariate calibration”, Journal of Chemometrics. 16:228–240 (2002)